



City Research Online

City, University of London Institutional Repository

Citation: Kiarad, H., Memarpour, M. M., Soltanieh, S. & Mergos, P. (2025). Seismic Vulnerability Assessment of Skewed Concrete I-girder Bridges Considering Various Structural Systems. Sustainable and Resilient Infrastructure, pp. 1-28. doi: 10.1080/23789689.2025.2540129

This is the accepted version of the paper.

This version of the publication may differ from the final published version.

Permanent repository link: <https://openaccess.city.ac.uk/id/eprint/35540/>

Link to published version: <https://doi.org/10.1080/23789689.2025.2540129>

Copyright: City Research Online aims to make research outputs of City, University of London available to a wider audience. Copyright and Moral Rights remain with the author(s) and/or copyright holders. URLs from City Research Online may be freely distributed and linked to.

Reuse: Copies of full items can be used for personal research or study, educational, or not-for-profit purposes without prior permission or charge. Provided that the authors, title and full bibliographic details are credited, a hyperlink and/or URL is given for the original metadata page and the content is not changed in any way.

City Research Online:

<http://openaccess.city.ac.uk/>

publications@city.ac.uk

Seismic Vulnerability Assessment of Skewed Concrete I-girder Bridges Considering Various Structural Systems

H. Kiarad^a, M.M. Memarpour^b, S. Soltanieh^c, P.E. Mergos^{c*}

^a Department of Civil Engineering, Imam Khomeini International University, Qazvin, Iran

^b Department of Civil Engineering, Faculty of Engineering and Technology, Imam Khomeini International University, Qazvin, Iran

^c Department of Civil Engineering, CITY ST GEORGE'S, University of London, Northampton Square, London EC1V 0HB, UK

Abstract

Variation in the type of structural system (bent-to-deck connection) not only significantly impacts the seismic performance of regular bridges but also adds complexity when skewness irregularity is involved. Previous studies have separately evaluated the impact of either the type of structural system or skewness on the vulnerability assessment of bridges. The present study examines, for the first time, the combined effects of structural systems and skew angles on the seismic response of multi-span reinforced concrete I-girder bridges. For this purpose, two prevalent superstructure systems, namely, multi-span simply supported and multi-span continuous, are considered. For each system, the boundary condition at superstructure-substructure interface is modeled assuming elastomeric bearings with steel dowels. In the case of the multi-span continuous system, two more commonly applied types of bent-to-deck connection are considered, including pinned connectivity and elastomeric bearings without steel dowels. To account for the irregularity, five skew angles ranging from 0° to 60° are also considered. Probabilistic seismic demand models are developed for key components, such as columns and bearings, and subsequently, component- and system-level fragility curves are generated. It is observed that superstructure skewness may reduce the sensitivity of column response to variations in the structural bridge systems by up to six times compared to regular counterparts. The results also reveal that skew angle variation can influence the bridge system fragility by up to 40% across different structural systems.

Keywords: Concrete I-girder bridge; Skewness; Structural irregularity; Fragility curves; Seismic vulnerability assessment

1. Introduction

Recently, there has been a controversial issue regarding the extent to which employing different types of structural systems affects the seismic response of highway bridges (Sun et al. 2023). In bridges, the load transition path between the superstructure and substructure is affected by the type of pier-to-bent connection (Ishac and Mehanny 2016). Consequently, it is imperative to assess the influence of various structural systems and connections on the seismic response of bridge. Several studies can be found in the literature that investigate the impact of different structural systems on a bridge under seismic excitations (Abdelnaby et al. 2014; Abbasi and Moustafa 2017; Abbiati et al. 2018). For example, Hou et al. (2017) investigated the seismic demand of simple-made-continuous I-girder bridges with integral abutments using three types of bent-to-deck connectivity: roller, pinned, and fixed. With the intention of minimizing moment demand at pier base of the bridge, the pinned and roller bent-to-deck connections were found to be preferable to the fixed connection in the skewed-only configurations in low-intensity seismic zones. A recent study by Sun et al. (2023) examined two types of connection between the pier and bent on a small-radius curved bridge: one with a monolithic pier-to-bent connection and the other with a fixed support installed at the pier-to-bent connection. They observed that the bridge model employing the latter structural system displays greater susceptibility to concrete splitting failure during seismic excitations in comparison to that of the former one. However, previous studies did not specifically address the effects of various structural systems, including multi-span simply supported and multi-span continuous, on the seismic vulnerability assessment of seismically-designed concrete I-girder bridges with seat-type abutments.

* Corresponding author.

E-mail address: panagiotis.mergos.1@city.ac.uk

Furthermore, in the latter system, they did not investigate the effects of bent-to-deck connections, including pinned connectivity and elastomeric bearings without steel dowels.

On the other hand, skewed bridges are widely acknowledged as the best solution to deal with the geometric restrictions associated with some regions in which regular (straight) configurations cannot be accommodated due to complex terrain (Miner 2014). Such situations necessitate adopting bridges with skew-angled bent and/or seat-type abutment in order to overcome the geometrical constraints or in other sense costly construction and easing traffic flow. In addition, the shift from a regular bridge to an irregular one, characterized by skew angles exceeding 20° (Caltrans 2019), inherently adds to complexities of the seismic assessment problems. For example, large earthquakes such as Chile (2010) resulted in deck unseating or displacement of superstructure, particularly evident in skewed bridges (Elnashai et al. 2012).

Over the last 25 years, many researchers have extensively studied the seismic behavior of skew bridges (Sullivan and Nielson 2010; Kaviani et al. 2012; Zakeri et al. 2014; Yang et al. 2015; Omranian et al. 2018; Abbasi and Moustafa 2019; Aldea et al. 2021). Their focus has been on the seismic assessment of skewed bridges, aiming to uncover vulnerabilities related to the structural components of bridge. Generally, it is observed that increasing the skew angle of bridge superstructure alters the seismic behavior of reinforced concrete (RC) bridges as a result of coupling translational modes with rotational mode of vibration. Through cloud analysis, Noori et al. (2019) evaluated the seismic vulnerability of a skewed two-span RC I-girder bridge with pinned bent-to-deck connection. It was indicated that as the skew angles vary from 0° to 60° , the seismic fragility of the column has been mitigated. In a study conducted by Huo and Zhang (2013), the seismic performance of RC highway bridges was perused under the combined effects of pounding and skewness. Their findings showed that when pounding did not occur, the seismic performance of the columns in skewed bridges outperformed that of straight bridges as the skew angle increased. Notwithstanding the extensive research on skewed bridges, none of the aforementioned works specifically inspected how various structural systems affect the seismic vulnerability assessment of skewed I-girder bridges.

The novelty of this research is to evaluate the simultaneous effects of structural systems and skew angles on the seismic response of RC I-girder bridges. In the present research, four unique combinations of superstructure systems and bent-to-deck connections are generated. To this end, two types of commonly used bridge superstructure systems, including multi-span simply supported I-girder and multi-span continuous I-girder, are studied. Additionally, two commonly applied connections in the case of continuous I-girder superstructure, namely, pinned connectivity and plain elastomeric bearings (also referred as unreinforced elastomeric bearings or elastomeric bearings without steel dowels), are considered. In addition, the angle of skewness varies between 0° to 60° with increments of 15° . Therefore, 20 different structural configurations of I-girder bridges are generated. For nonlinear time history analysis (NLTHA), finite element models of the bridges are created, and a set of bidirectional horizontal far-field ground motions is selected. A total of 800 NLTHAs are conducted on the bridge models using the OpenSEES platform. To compare seismic vulnerability of the most important components, such as columns and bearings, fragility assessment is implemented at four different limit states by developing probabilistic seismic demand models for each bridge model. Subsequently, the system-level fragility of all bridge models is derived through joint probabilistic demand models. Lastly, this paper ends with notable findings and recommendations for future research.

2. Structural systems

In this research, different types of structural systems applied to concrete I-girder bridge are studied based on their capabilities in transferring loads between the super- and substructure. Two commonly used types of bridge superstructure systems are studied: multi-span simply supported I-girders (MSSS) and multi-span continuous I-girders (MSC). The MSSS and MSC structural systems are distinguished by the presence of a gap between adjacent decks at the bents for the former case. The MSSS structural system entails discrete spans with joints, allowing each span to act independently in response to seismic loads. In contrast, in the MSC superstructure, the bridge spans are connected without any expansion joints. For each system, the boundary condition at superstructure-substructure interface is modeled assuming elastomeric

bearings with steel dowels. Additionally, two prevalent connectivity types in MSC superstructures are examined: pinned connectivity and plain elastomeric bearings. Overall, the structural systems are categorized as multi-span simply supported (MSSS) (Ghosh 2021; Bhaskar Panchireddi and Ghosh 2023), multi-span continuous with fixed and expansion bearings (MSC-FEB) (Yang et al. 2015; Ghosh 2021), multi-span continuous with elastomeric bearings (MSC-B) (Zakeri and Ghodrati Amiri 2014; Mirzai et al. 2023), and multi-span continuous with pinned connectivity (MSC-PC) (Soltanieh et al. 2019). Fig. 1 provides a general view of the various structural systems for multi-span RC I-girder bridges. To simplify notation, each case of the structural systems is denoted by the letter 'C' with a numerical subscript. Accordingly, MSC-PC (no fixed/expansion bearings at bents), MSC-FEB, MSSS, and MSC-B are indicated as C_1 , C_2 , C_3 , and C_4 hereafter. The four structural systems and their corresponding designations are summarized in Fig. 1.

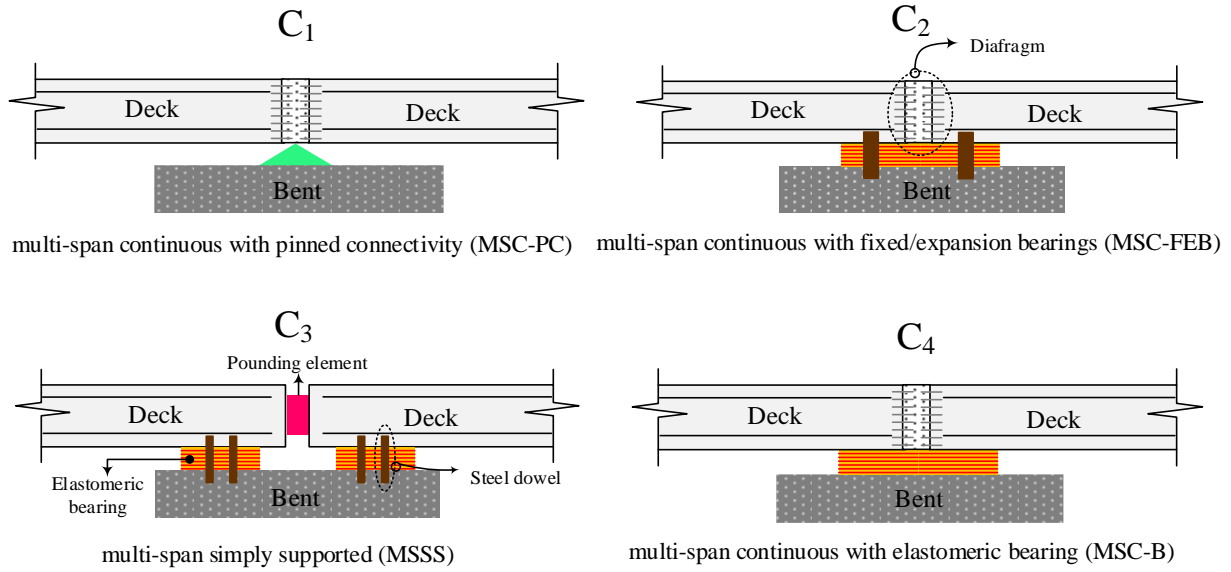


Fig. 1. General view of the various structural systems for multi-span I-girder bridge, with associated designations

The way in which loads are transferred between the superstructure and substructure of bridges is heavily influenced by the type of structural system. The C_1 structural system allows free relative rotation between the superstructure and the substructure about all axes at the bent. In other words, this structural system transfers all translational forces from the superstructure (deck girders) to the substructure (cap beam) without moment transfer. In the case of C_4 , there is no moment transfer between the superstructure and the substructure at the bent either, and the seismic translational loads transfer via bearings. Although the seismic load path for both the C_2 and C_3 systems is similar to that of the C_4 structural system, the movement of the superstructure of the two former systems is restricted by steel dowels. This occurs once the steel dowels engage with the elastomeric bearing.

3. Models of bridges

3.1. Bridge geometric characteristics

Multi-span I-girder reinforced concrete (RC) bridges are a widely-constructed structural design found across the globe (Jankowski 2015; Kabir et al. 2019; Shekhar et al. 2022). A schematic view of longitudinal elevation and transverse cross-section of the bridge, as well as the arrangement of bearing types across various structural systems is represented in Fig. 2. The bearing types are identified by distinct symbols: fixed bearing (orange triangle), expansion bearing (green circle), bearing without steel dowels (pink circle), and pinned connection (blue triangle). The bearing characteristics are discussed in §3.2. The superstructure has a length of 48.8 m and a width of 15.01 m. The superstructure is composed of a middle

span with length of 24.4 m, and two side spans with length of 12.2 m. The bridge deck is constituted of eight concrete girders and a concrete slab on top with a thickness of 0.178 m. AASHTO girder types of I and III girders are used for the side spans and middle-span. The side spans are supported by seat-type abutments at one end and a three-column bent at the other. The abutments rest on batter and vertical-type pile foundations, while the bent is attached to three eight-pile foundations. Backwall with a height of 2.4 m is accounted for embankment. Clayey backfills are also assumed for the abutment backwall. Typically, the gap between abutment and deck is 25.4 mm, while the gap between adjacent decks is 38.1 mm.

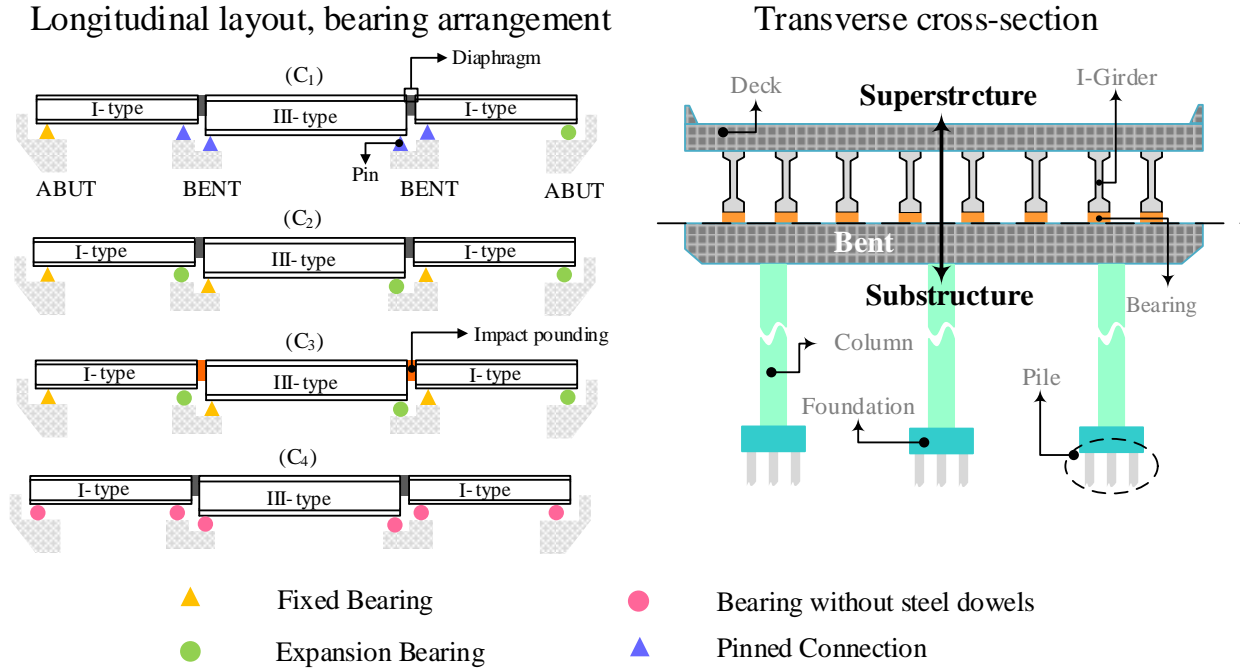


Fig. 2. Schematic view of a typical multi-span RC I-girder bridge with bearing distribution across structural systems

Columns of the bridge have a circular section with a diameter of 0.914 m and a height of 4.6 m. They are connected at the top using a cap beam of rectangular section with a width of 1.07m and depth of 1.22 m, as the columns are also tied at the bottom using a pile cap. The center-to-center distance of columns at bent is 5 m. This circular column comprises 12 #29 longitudinal rebars. Moreover, #13 stirrups with a spacing of 76 mm on center (#13 bars @ 76 mm o.c.) are transversely distributed along the column, resulting in a ductile column (Ramanathan et al. 2012). This implies seismically-designed columns, whereby the flexural mode predominates in the column. Cross-section and elevation view of the seismically designed reinforced concrete bridge column are illustrated in Fig. 3.

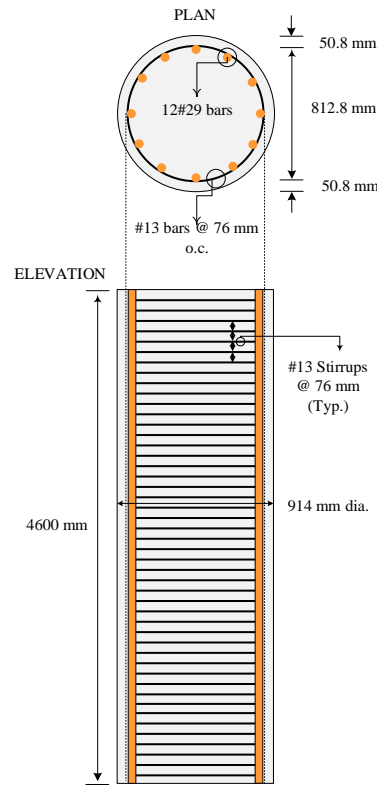


Fig. 3. Cross-section and elevation view of the seismically designed reinforced concrete bridge column

It should be noted that only neoprene pads (elastomeric bearings) are used in the C₄ structural system without any steel dowels beneath the concrete girders, whereas the concrete girders of the three other structural systems are integrated into elastomeric bearings utilizing steel dowels, i.e., fixed and expansion bearings. The fixed and expansion bearings are constructed by embedding two steel dowels with a diameter of 25.4 mm above the concrete cap beam and/or abutment. It is done by passing the steel dowels through the circular holes within the elastomeric bearings for the fixed bearings and slotted holes for the expansion bearings. The dimensions of the slotted hole are 31.8 mm x 76.2 mm, and the diameter of the circular hole is 31.8 mm. Moreover, the steel dowel must be inserted into a 76.2 mm hole in the bottom of the girder such that the steel dowel can move loosely inside the hole. In the case of I-type girders, the elastomeric bearing pads are 406 mm wide and 152 mm long with a thickness of 25.5 mm. In the case of III-type girders, the dimensions are 559 mm x 203 mm x 25.5 mm. The only difference between the fixed and expansion bearings is a gap between the elastomeric bearing pad and the steel dowel, which is 3.2 mm and 25.4 mm, respectively, along the longitudinal axis. In contrast, an identical gap size of 3.2 mm is considered for both types of bearings along the transverse direction.

The geometric configuration of the bearings and the steel dowel holes are illustrated in Fig. 4. Because the deck is prone to unseating during seismic events, the steel dowels serve as restraining devices to prevent excessive movement of the girders that are seated on elastomeric bearings. Besides, to protect the bridge from potential movements such as anticipated thermal expansion, gap-defined holes are implemented to relieve stresses in the bent/abutment (Maleki 2005). In total, 96 steel dowels resided in 48 elastomeric bearing pads throughout the bridge where the superstructure meets the supports for C₃ and C₂. Similarly, in the same order, 32 steel dowels and 16 elastomeric bearing pads are needed for C₁, whereas only 48 elastomeric bearing pads are required for C₄. When the steel dowel acts elastically, the combination of the steel dowel and elastomeric bearing restricts the motion of girders. If the steel dowel breaks under strong dynamic excitation, the only governing factor between the girder and bearing is sliding due to the elastomeric bearing. Furthermore, such bearings are immune against walking out, contingent on being properly secured in place. Detailed information about the geometric properties of the bridge can be found in (Nielson 2005).

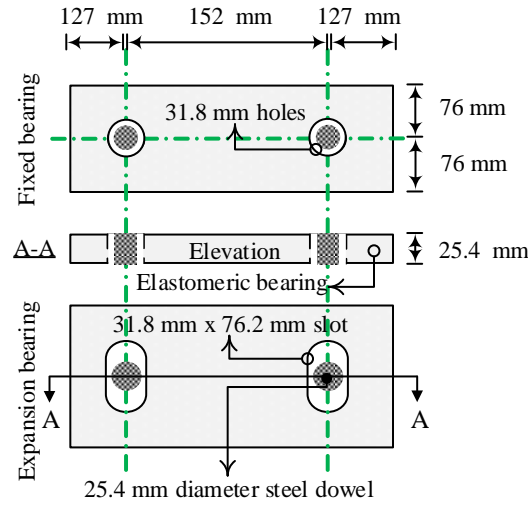


Fig. 4. Plan and elevation view of the fixed and expansion bearings with steel dowels

For implementing skewed geometry in the bridge, angular increments of 15° (ranging from 0° to 60°) are adopted (Mangalathu et al. 2019; Noori et al. 2019; Somala et al. 2021; Rezaei et al. 2025). Fig. 5 compares the bridge configurations with straight ($\theta = 0^\circ$) and skewed ($\theta \neq 0^\circ$) geometries.

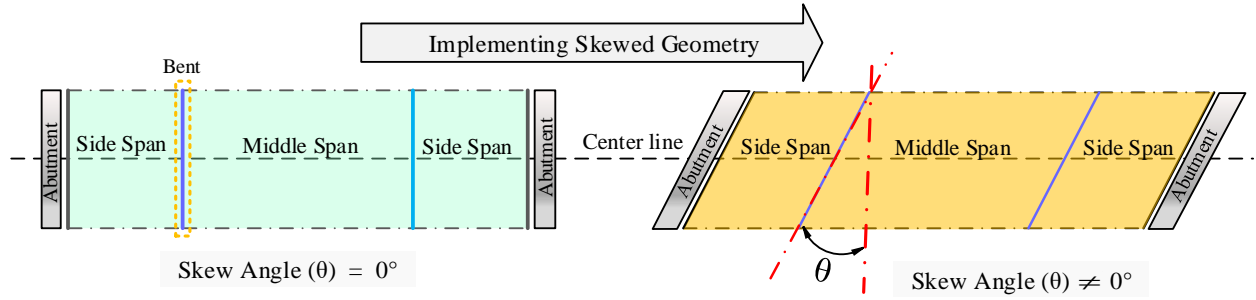


Fig. 5. Geometric configuration of the straight/skewed concrete I-girder bridge system

3.2. Finite element modeling

Nonlinear three-dimensional finite element models of the bridge are developed in OpenSEES (McKenna 2011). It is assumed that the superstructure remains elastic during seismic excitations. Therefore, the deck is modeled using elastic beam-column elements at center along the longitudinal direction. Geometric and mechanical properties of the deck are calculated and assigned to these elastic elements. Nodal mass is defined on superstructure nodes. The nonlinear behavior of columns is modeled by displacement-based beam-column elements and discretized fiber sections. The stress-strain laws of materials used to model confined and unconfined concrete are based on the work of Terzic and Stojadinovic (2015), and the maximum compressive strength is calculated by means of equations proposed by Mander et al. (1988). In OpenSEES, both the confined and unconfined behaviors are modeled using Concrete01 in which the ultimate concrete compressive strains are 0.062 and 0.0055. Besides, reinforcing steel is modeled using Steel01. At the top of the columns, the bent is modeled using a nonlinear beam-column element and a quadrilateral fiber section. The foundation system at the bottom of the columns is also simulated by means of linear translational and rotational springs. In abutments, it is important to note that the piles and the surrounding soil both participate in passive resistance, whereas the piles alone contribute to the active resistance. Additionally, the transverse direction resistance is only provided by piles without taking into account the resistance of wing walls. According to Shamsabadi et al. (2014), the HyperbolicGap material is used to model the nonlinear behavior of the abutment back-wall soil. To simulate piles, a trilinear model recommended by Choi (2002) is adopted. Furthermore, an impact element is defined through a bilinear model for deck-to-deck/deck-to-abutment collisions according to the recommendation of Muthukumar and DesRoches (2006). The energy dissipation of pounding is also considered in the model. A schematic view

is presented in Fig. 6 illustrating the arrangement and behavior of all the components utilized in the analytical model of the bridge in OpenSEES.

The fixed and expansion bearings are composed of an elastomeric bearing and two steel dowels. Seven steps are involved in the modeling of these bearings. Step 1: the elastomeric bearings associated with I-girder and III-girder are modeled using an elastic perfectly-plastic material that has an initial stiffness of 3.4 kN/mm and 6.2 kN/mm, respectively. Step 2: the behavior of the steel dowel is modeled using a hysteretic material with an initial stiffness of 92 kN/mm. Step 3: to account for the gap in the bearings, an elastic perfectly-plastic gap material with an initial stiffness of 92 kN/mm is defined. Then, the hysteretic material modeled in step 2 is connected in series to the elastic perfectly-plastic gap material with a positive initial gap, e.g., +3.2 mm for the longitudinal fixed bearing, resulting in the tension behavior of the steel dowel considering the positive gap. Step 4: step 3 is repeated with a negative initial gap, in order to achieve the compression behavior of the steel dowel considering the negative gap (-3.2 mm). Step 5: through the parallel connection of the systems of spring created in steps 3 and 4, the cyclic behavior of steel dowels considering two-sided gaps is modeled. Step 6: the hysteretic behavior of the longitudinal fixed bearing is made by combining in parallel the resulting system of springs from step 1 with that of step 5. Step 7: the resultant material generated in step 6 is applied to a zero-length element connecting the nodes between the deck and bent/abutment. The expansion bearing is also modeled in a similar way to the fixed bearing.

As mentioned in §3.1, the only difference between fixed and expansion bearings is the size of the gap at which the steel dowels can freely move until the closure of the gap. Once the gap in the fixed and expansion bearings is closed, engagement between the steel dowel and elastomeric bearing is incurred. Consequently, this engagement is postponed by the time delay associated with the size of the gap. In this research, interaction between steel dowels and elastomeric bearings is overlooked.

In C_1 , translational degrees of freedom (DOFs) of the super- and substructure nodes are equalized while the rotational DOFs are free to rotate. In the modeling of the others, such as C_2 , only the vertical translational direction DOF of the superstructure node is equalized to that of the cap beam, and the rotational DOFs can rotate freely. In case of C_2 and C_3 , the deck is connected to the cap beam using a zero-length element and the materials defined earlier in this section (i.e., fixed and expansion bearings). Furthermore, C_4 is quite similar to C_2 with the only difference that steel dowels are eliminated in the model of C_4 . It should be noted that in seat-type abutments, the gap and the pounding between the superstructure deck and the abutment need to be addressed correctly. In this manner, the longitudinal bearings are deployed parallel to the impact element in the abutment as well as in series with the soil element. The placement of bearing types along the bridge length can be seen in Fig. 2.

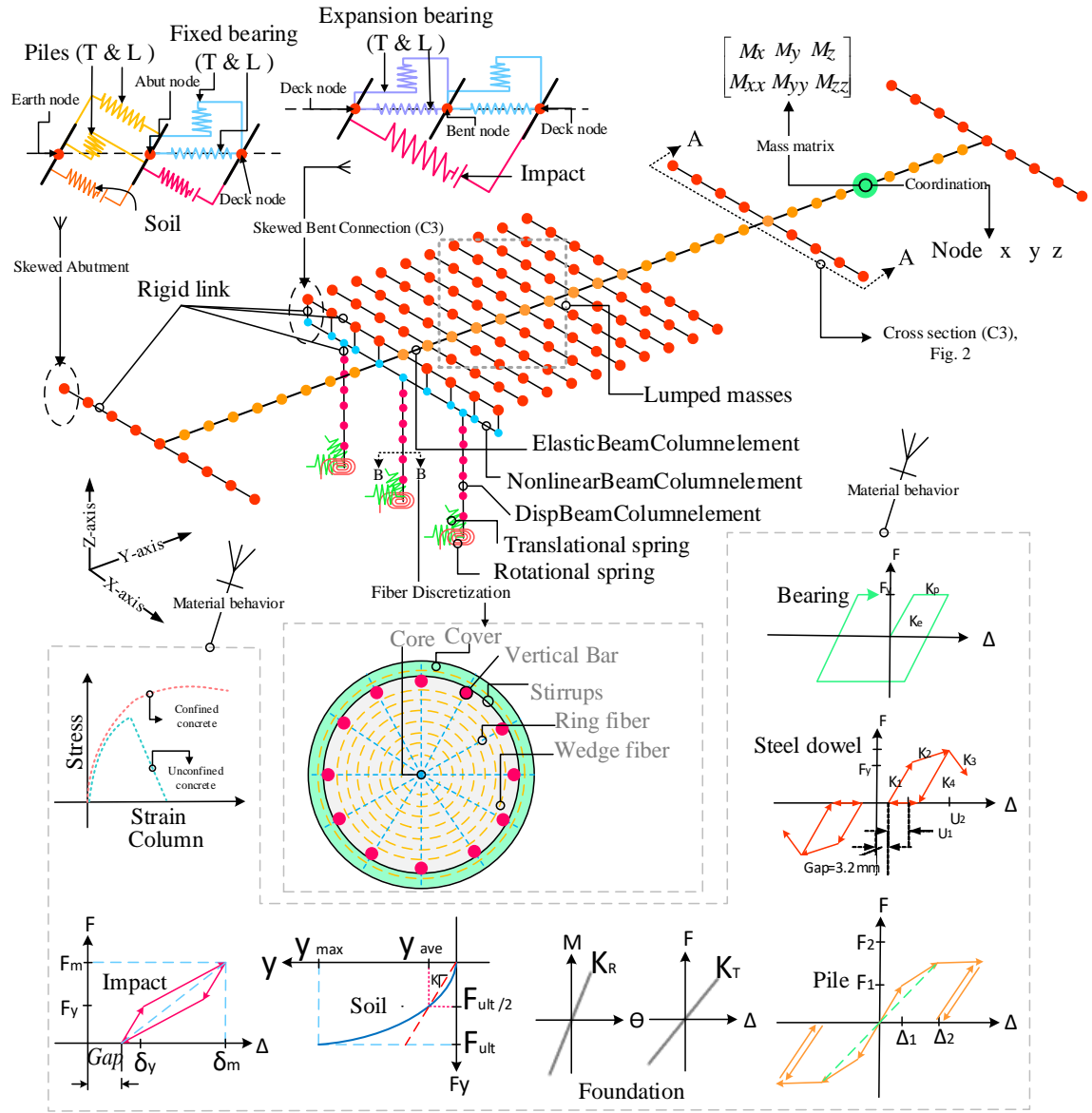


Fig. 6. Analytical model of bridge

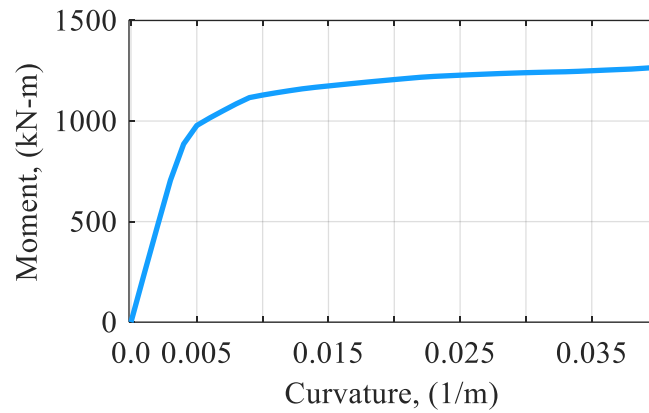


Fig. 7. Pushover analysis on column along longitudinal direction (Monotonic moment-curvature behavior of column)

A pushover analysis is conducted on the three-dimensional finite element model of the straight bridge assuming C₁. Fig. 7 illustrates the monotonic moment-curvature behavior of the circular fiber-defined section of the column along the longitudinal direction. A cyclic analysis is also conducted in order to demonstrate the cyclic behavior of the column and bearings. Relationship between moment and curvature of the column can be seen in Fig. 8a. The hysteretic behavior of the force-deformation related to the longitudinal fixed and expansion bearings is also illustrated in Figs. 8b and c, respectively.

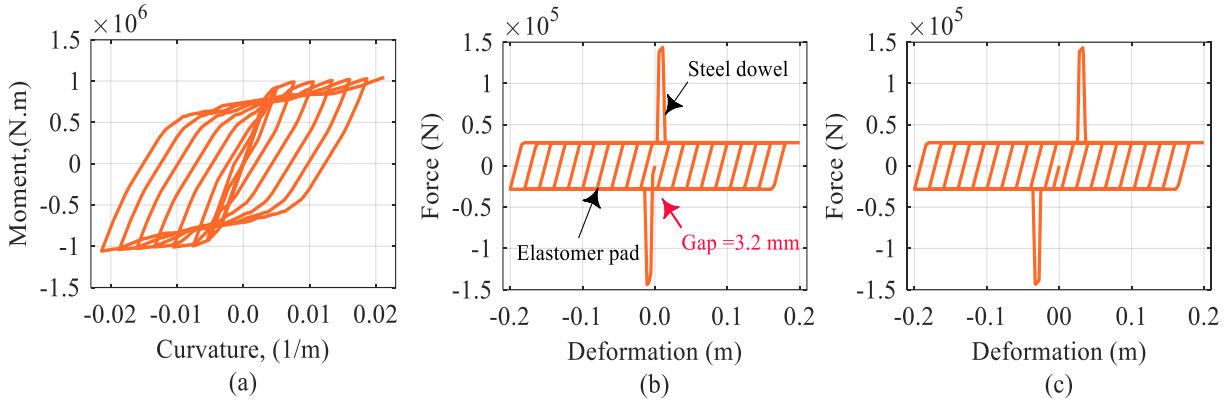


Fig. 8. Cyclic analysis response along longitudinal axis for (a) moment-curvature relationship of column, (b) fixed bearing, and (c) expansion bearing

As opposed to straight bridges, skewed bridges are built with skewed-angle bents and/or seat-type abutments. In this regard, finite element models of skewed bridges contain additional rigid elements along the transverse axis to account for skewness effects on seismic responses of bridges. The transverse deck elements are rotated in accordance with the desired skew angle of the bridge, which produces an angle of θ other than 90° with respect to the longitudinal deck elements (i.e., parallel to the traffic direction). Additionally, the implementation of skew angles into the finite element models necessitates alterations to the orientation of several bridge elements. These elements are related to the piles and their surrounding soil, including impact, soil, and pile springs at the abutments, and rotational and translational springs at the foundation. These elements are required to be adjusted in accordance with the implemented skew angle of the bridge. For modeling skewed C₃ bridges, the orientation of the impact element at adjacent decks is also modified such that it is normal to the decks. Nonetheless, all bearings, including the fixed and expansion bearings as well as the bearings without steel dowels, remain unchanged for models across all skew angles such that their orientations are collinear with the bridge principal axes.

The deck of skewed bridges under seismic excitation tends to rotate in-plane about its vertical axis and subsequently, the skewed superstructure separates from the abutment at the acute corner while binding at the obtuse corner. This phenomenon leads to the creation of an inherently-asymmetric passive wedge inside the abutment backfill (Shamsabadi and Rollins 2014). In addition, the volume of backfill soil mobilized per unit length of the abutment wall increases from the obtuse corner to the acute corner. For analytical model of the skewed abutments to reflect these effects, different properties must be assigned to the nonlinear hyperbolic springs depending on their distance from the obtuse corner. The illustration of the analytical model related to skewed-angle abutments can be found in Fig. 9. To consider the different properties in the soil springs, the variation coefficients of soil stiffness are calculated based on $\beta=0.3(\tan(\theta)/\tan(60^\circ))$, which are a function of the skew angles (Kaviani et al. 2012), and are postulated at both abutments during the skewing process. In skewed bridges, there is also the potential for the decks to rub against each other due to the addition of skew, but in the simulation process, this can be ignored assuming the frictional resistance is substantially lower than the impact stiffness of the surfaces (Johnson et al. 2006). In this study, five different skew angles of 0° , 15° , 30° , 45° , and 60° are selected to investigate the skewness impacts on seismic responses of RC I-girder bridges. Each case of skew angles is represented by the letter 'S' with a numerical subscript for simplicity. Hereafter, S₁ to S₅ are representatives of 0° to 60° angles of skew with increments of 15° . It should be noted that structural responses are influenced by

modeling assumptions (Engen et al. 2017; De Matteis et al. 2022). For example, the consideration of an inherently asymmetric passive wedge within the abutment backfill for skewed bridges is one of such modeling assumptions adopted in this study.

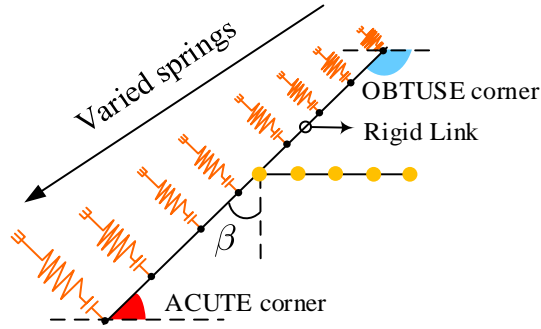


Fig. 9. Soil springs simulation for skewness

Damping proportional to the stiffness component using the updated tangent stiffness is utilized in the models in which only one mode, the first mode, is assigned to determine the damping coefficients. In the models, a 5% damping ratio is assumed. In the present study, seismic excitations are imposed on the fixed nodes of the soil springs (i.e., HyperbolicGap elements) at the abutment and the bent foundation springs (i.e., linear translational and rotational elements).

4. Dynamic bridge characteristics

The dynamic characteristics of the bridge models with the different structural systems and skew angles are determined through eigenvalue analysis. The periods of the first and the second modes of vibration are presented in Table 1 for the 20 bridge models. In the table, C_2S_3 denotes the bridge model with the MSC-FEB structural system (C_2) and a skew angle of 30° (S_3). This table shows that the elastic period of the first vibration mode is longer than that of the second vibration mode for all the models. The fundamental mode of a straight bridge is characterized by a mode shape that is predominantly in the longitudinal direction.

According to the table, the fundamental periods for the regular realizations of the bridge models are 0.548s, 0.559s, 0.635s, and 0.559s corresponding to C_1 , C_2 , C_3 , and C_4 , respectively. The bridge model with the C_1 structural system is inherently stiffer than the bridge model with discontinuous superstructure and fixed/expansion bearings, C_3 , in which the fundamental period is the highest amongst the structural systems. In the case of C_1 , C_2 , and C_4 with S_1 , the second mode shape oscillates in the transverse direction. However, the second mode shape of C_3S_1 exhibits side spans vibrating in both rotational and translational DOFs, while its middle span sustains significant translational motion only. Referring to the table, the periods of 0.373s, 0.435s, 0.484s, and 0.435s correspond to the second modes of C_1S_1 , C_2S_1 , C_3S_1 , and C_4S_1 .

Table 1

Periods (s) of the first and the second modes of vibration

		Skew angles									
		S_1		S_2		S_3		S_4		S_5	
		1 st	2 nd	1 st	2 nd	1 st	2 nd	1 st	2 nd	1 st	2 nd
Structural systems	C_1	0.548	0.373	0.548	0.373	0.548	0.373	0.549	0.373	0.550	0.374
	C_2	0.559	0.435	0.572	0.445	0.573	0.445	0.574	0.445	0.575	0.445
	C_3	0.635	0.484	0.646	0.488	0.659	0.484	0.670	0.480	0.670	0.477
	C_4	0.559	0.435	0.572	0.445	0.573	0.445	0.574	0.445	0.575	0.445

The influence of skewness on the mode shape of the bridge can be easily understood from the periods of vibration for the first and the second modes provided in Table 1. For instance, in the C_3S_4 model, the first mode period is 0.67s, whereas it is 0.63s for C_3S_1 . Unlike C_3S_1 , the first mode shape of C_3S_4 is a

combination of longitudinal and transverse movements. Nevertheless, the second mode shape of C_3S_4 , albeit for middle span is translational along the 45° -transverse axis of the bridge akin to that of the C_3S_1 model. However, the side spans of the C_3S_4 model demonstrate an interaction of the translational and rotational movements. Besides, the second mode periods of vibration of the straight and skewed bridges with C_3 are approximately equal, as seen with cases of C_1 , C_2 , and C_4 . Overall, the skewed bridges show complex interaction between the first and the second modes of vibration in comparison to the straight bridges where the first mode of vibration is normally along the longitudinal direction of the bridge, and the second mode of vibration is along the transverse direction.

5. Seismic fragility function methodology

5.1. Fragility function

Following Nielson (2005) and Mangalathu et al. (2019), this study employs fragility functions to generate fragility curves. Numerous researchers have employed analytical fragility functions to assess the seismic vulnerability of skewed RC I-girder bridges (e.g., Soleimani et al. 2017; Mangalathu et al. 2019). This paper also evaluates, in an analytical manner, the vulnerability of bridge components across different structural systems and angles of skewness. The seismic fragility function estimates the likelihood of bridge component demand reaching or exceeding a predetermined threshold at a certain level of seismic intensity. As a general description of fragility function (conditional probability), it can be stated as follows:

$$Fragility = P\left\{\frac{D}{C} \geq 1 \mid IM\right\} \quad (1)$$

Where P is the probability that the seismic demand on a bridge component (D) meets or exceeds its corresponding quantified limit state capacity (C) subject to a given level of intensity measure (IM). To make it more convenient, this probability is transformed into the space of the log-normal probability distribution (Wen et al. 2003).

Based on Eq. (1), the fragility function is evaluated through a convolution of capacity models, given a limit state, and demand models. IM -conditioned demand models are probability distributions of structural demand, known as probabilistic seismic demand models (PSDM). To develop PSDMs, peak responses of structural demands or engineering demand parameters ($EDPs$) obtained through NLTHAs are plotted versus the values of ground motion IM (e.g., peak ground acceleration). Then, utilizing the IM - EDP pairs and a power-law function proposed by Cornell et al. (Cornell et al. 2002), a linear regression of $EDPs$ on IMs is established to form PSDMs. Having the PSDMs, the logarithmic correlation between the median estimate of engineering demand parameter (S_D) and IM can be established as given in Eq. (2):

$$\ln(S_D) = \ln(a) + b \ln(IM) \quad (2)$$

The equation above approximates S_D as a function of IM values. In addition, $\ln(a)$ and b represent coefficients of the linear regression fitted to given pairs of EDP - IM . The model parameter $\ln(a)$ is the vertical intercept and the parameter b is the slope. The scatter plot of the PSDM portrays the relation between $EDPs$ and IMs in a log-normal space for each component (e.g., see Fig. 12a).

The logarithmic standard deviation of S_D conditioned on IM , $\beta_{D/IM}$, is expressed in the following way with respect to the basic statistical formula:

$$\beta_{D/IM} = \sqrt{\sum_{i=1}^N [\ln(EDP_i) - \ln(S_D)]^2 (N-2)^{-1}} \quad (3)$$

Where N is the number of ground motions, and EDP_i is peak demand obtained from NLTHA corresponding to i^{th} ground motion. $\beta_{D/IM}$ is also termed as ‘dispersion’, that is a dimensionless quantity.

After estimating the demand parameters, S_D and $\beta_{D/IM}$, and adopting capacity model, S_C and β_C , seismic fragility curves of bridge components conditioned on IM are generated using the following equation:

$$P\{D \geq C | IM\} = 1 - \Phi \left[\frac{\ln(S_C) - \ln(S_D)}{\sqrt{\beta_{D/IM}^2 + \beta_C^2}} \right] \quad (4)$$

where $\Phi[\cdot]$ indicates the standard normal cumulative distribution function, S_C and β_C represent the median and dispersion of the capacity model, which is elaborated in (§5.3).

System-level fragility of bridges can be assessed by integrating component-level fragility curves through the development of joint probabilistic seismic demand models (JPSDMs) (Nielson 2005; Mangalathu et al. 2019). The JPSDM accounts for correlations between component demands. If $Z = (Z_1, Z_2, \dots, Z_n)$ denotes the vector of demands on the n components of bridge in the original space, then $B = \ln(Z)$ represents the corresponding vector of component demands in log-transformed space. The JPSDM is formulated by assembling the mean vector, μ_B , and covariance matrix, σ_B , in the transformed space. The correlation coefficients between component demands are obtained from NLTHA results. Monte Carlo simulation is employed to generate 10^6 realizations of demand and capacity, enabling probabilistic estimation of demand exceeding capacity for each IM value. This process is repeated for increasing IM values, and regression analysis is used to derive the lognormal parameters (median and dispersion) defining the bridge system fragility curve.

5.2. Earthquake ground motion suite

To obtain the seismic response of bridge components in a probabilistic manner, a set of 40 unscaled standardized ground motions is selected for NLTHAs. The broad-band ground motions were originally proposed by Baker et al. (2011) for the Transportation Systems Research Program PEER (TSRP). The horizontal response spectra of the set correspond to the median and logarithmic standard deviations predicted for a strike-slip earthquake with a magnitude of 7 on the Richter scale ($M_w = 7$) and a seismic source-to-soil distance of 10 km. An average shear wave velocity of 250 m/s has been assumed at a depth of 30 meters above the soil layer. The ground motion set accounts for aleatoric uncertainty (record-to-record variability). Various factors may contribute to such uncertainty including the frequency content of ground motions, earthquake magnitudes, and the distance between source and site (Tehrani and Mitchell 2013). It should be noticed that the orthogonal horizontal pairs of the selected ground motions were mathematically rotated into their fault-normal (FN) and fault-parallel (FP) orientations. Accordingly, they are simultaneously applied to the principal axes of the bridge model in order to perform NLTHAs (e.g., Mangalathu et al. 2019; Noori et al. 2019).

5.3. Limit States

For the development of the fragility function, it is equally important to define limit states of the bridge components (capacity model) as it is to formulate the demand model. Depending on the functional level of the bridge components, the quantity of limit states is determined. Prescriptive approaches based on physics assumptions are used in this process. Four qualitative descriptions of the limit states are apparent; slight, moderate, extensive, and complete. These definitions correspond to those provided by HAZUS qualitative limit states (FEMA 2003).

Seismic vulnerability assessments mainly focus on two bridge components: columns and bearings. For this purpose, five *EDPs* are defined and used in this research, including curvature ductility demand, μ_ϕ , for columns, and displacement, δ , for longitudinal and transverse bearings. The limit state quantities for the seismically designed column are adopted from previous study in terms of curvature ductility (Howard Hwang et al. 2000; Ramanathan et al. 2012). Furthermore, the limit state values related to fixed and expansion bearings are adopted from (Ramanathan et al. 2012). Bearings without steel dowels follow the limit state values proposed in Ramanathan's thesis (2012). For simplicity, the same abbreviations are

adopted for both dowel-equipped and non-dowel bearings. Table 2 lists these components along with their median values (S_C) and includes the structural system types where these bearings are applied. The dispersion of capacity (β_C) is 0.25 for slight/moderate damage states and 0.47 for extensive/complete limit states.

To calculate μ_ϕ , the ratio of the maximum curvature (ϕ_m) to the yield curvature (ϕ_y) must be determined. Priestley et al. (1996) proposed a simplified equation to estimate column yield curvature (ϕ_y), which is a function of the cross-sectional diameter of the column and yield strain of the longitudinal reinforcement. In addition, ϕ_y is calculated using bilinear idealization as recommended by the same researchers. Actually, a decent agreement can be found between the two ($\phi_y = 0.00485$). It should be mentioned that the square root of sum of squares (SRSS) method is employed to capture the column response.

Table 2

Bridge *EDPs*, limit state thresholds, and associated structural systems

Component	Abbr.	<i>EDPs</i>	Units	Limit states				Structural system
				Slight	Moderate	Extensive	Complete	
				S_C	S_C	S_C	S_C	
Column curvature	Col	Curvature ductility (μ_ϕ)	-	1	5.1	7.5	9	C ₁ , C ₂ , C ₃ , C ₄
Longitudinal expansion bearing	LEB	Displacement (δ)	mm	30	100	150	255	C ₁ , C ₂ , C ₃
Transverse expansion bearing	TEB							C ₁ , C ₂ , C ₃
Longitudinal fixed bearing	LFB							C ₁ , C ₂ , C ₃
Transverse fixed bearing	TFB							C ₁ , C ₂ , C ₃
Elastomeric Bearing	-			25	100	150	255	C ₄

5.4. Efficient intensity measure

As described, record-to-record (RTR) variability of ground motions brings some levels of inherent randomness into seismic assessment problems (Ellingwood and Wen 2005; Tehrani and Mitchell 2013). To this end, the choice of an effective and optimal *IM* can significantly reduce the statistical variations caused by RTR variability. An efficient *IM*, which is just one of the determinants of an optimal *IM* (Giovenale et al. 2004), can minimize the variation in the estimated structural demand. Based on Eq. (3), the most efficient *IM* is determined by the lowest $\beta_{D/IM}$ value (dispersion) among the given *EDP-IM* pairs. This efficiency is explored among three *IMs* including peak ground acceleration (PGA), peak ground velocity (PGV), and spectral acceleration at the intermediate period of the first and second modes of vibration (S_a) (Baker and Cornell 2006). The geometric mean of the *IM* values for the two horizontal components of each ground motion is regarded as the resultant *IM* (Baker and Cornell 2006). For S_a , which is a structure-dependent *IM*, the geometric mean of S_a must also be estimated separately for each bridge model. The $\beta_{D/IM}$ values for the components of all the bridge models are calculated with respect to the three explored *IMs*. For instance, the $\beta_{D/IM}$ values associated with the column curvature ductility demand of all the models for the three *IMs* are offered in Fig. 10. In this study, PGA is chosen as the efficient *IM* because it showed the highest efficiency in most cases. This choice is also acknowledged by other researchers (e.g., Padgett 2008; Ghosh 2021).

The regression coefficients ($\ln(a)$ and b) and the coefficient of determination (R^2) are derived for the considered *EDPs* for the twenty models and three *IMs*. R^2 exhibits the accuracy of PSDMs, which is a dimensionless quantity. Figs. 11a and b show the R^2 estimates across the bridge components in the twenty bridge models. Based on the figure, the R^2 estimates for the most PSDMs associated with PGA are reasonable, indicating a relatively strong correlation between these *EDPs* and PGA.

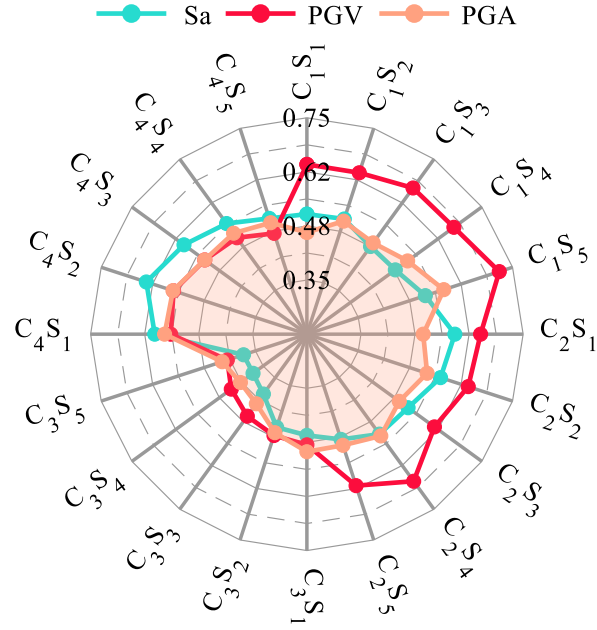


Fig. 10. Dispersion ($\beta_{D/IM}$) estimates for the three explored IMs considering column curvature ductility demand as *EDP* across all the bridge models

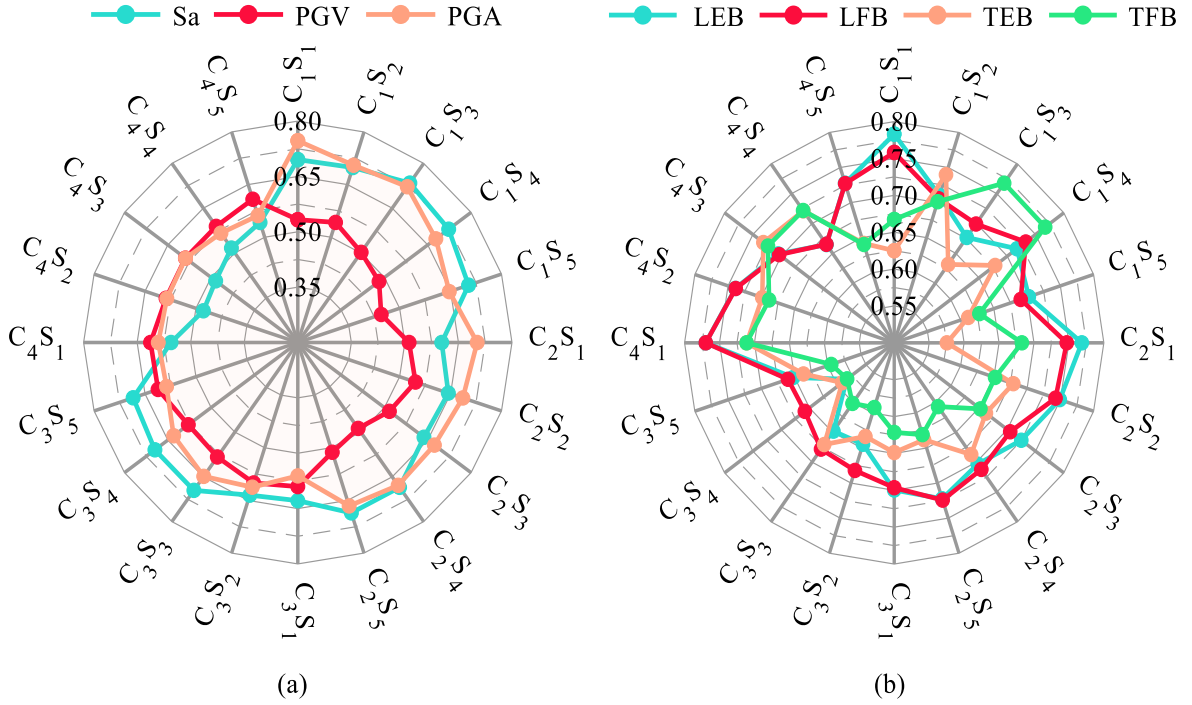


Fig. 11. Coefficient of determination (R^2) estimates for all bridge models for (a) column curvature ductility demand for three different *IMs*, (b) bearings for *PGA* as *IM*

A sample of PSDMs related to the column of the C_3S_3 model and the bearings of the C_3S_5 model are displayed in Figs. 12a and b, respectively. The probabilistic seismic demand parameters for the five *EDPs* of two bridge models, C_1S_1 and C_3S_3 , are also given in Tables 3-5 with respect to *PGA*, *Sa*, and *PGV* as *IM*, respectively. The tables list the probabilistic seismic demand parameters including $\ln(a)$, b , $\beta_{D/IM}$, and R^2 .

Table 3Probabilistic seismic demand parameters for bridge components considering PGA as *IM*

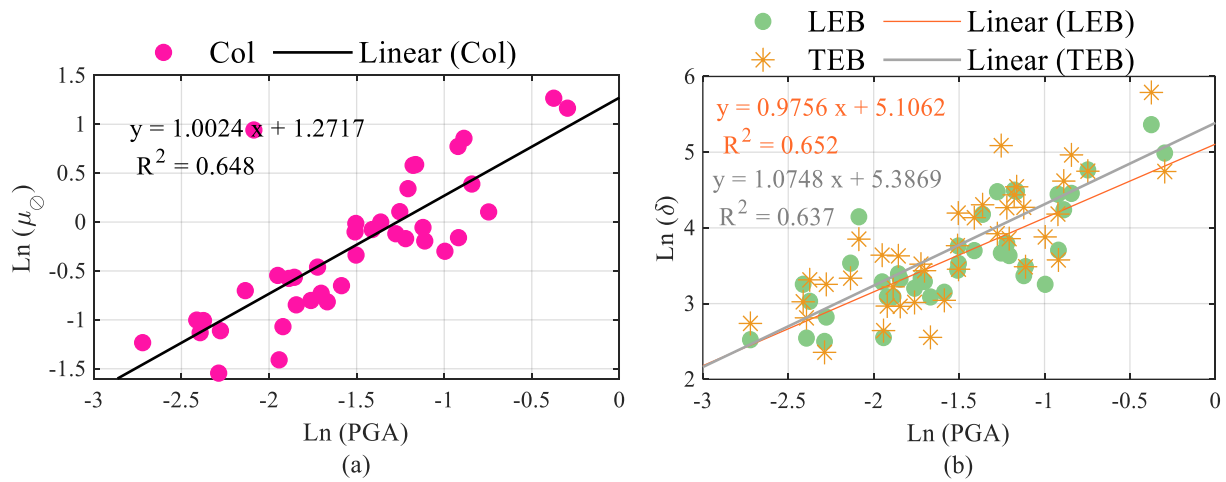
<i>EDPs</i>	<i>Models</i>							
	C_1S_1				C_3S_3			
	$\ln(a)$	b	R^2	$\beta_{D/IM}$	$\ln(a)$	b	R^2	$\beta_{D/IM}$
<i>IM</i> = PGA								
Col	1.88	1.38	0.74	0.46	1.27	1.00	0.64	0.42
LEB	5.78	1.31	0.78	0.40	5.33	0.99	0.64	0.42
LFB	5.88	1.38	0.75	0.75	5.72	1.43	0.67	0.57
TEB	4.54	1.17	0.62	0.53	5.64	1.63	0.67	0.66
TFB	4.90	1.34	0.66	0.55	5.52	1.57	0.60	0.74

Table 4Probabilistic seismic demand parameters for bridge components considering *Sa* as *IM*

<i>EDPs</i>	<i>Models</i>							
	C_1S_1				C_3S_3			
	$\ln(a)$	b	R^2	$\beta_{D/IM}$	$\ln(a)$	b	R^2	$\beta_{D/IM}$
<i>IM</i> = <i>Sa</i>								
Col	0.78	1.24	0.69	0.51	0.55	0.94	0.69	0.39
LEB	4.73	1.18	0.72	0.45	4.60	0.92	0.66	0.41
LFB	4.78	1.26	0.71	0.49	4.73	1.40	0.77	0.48
TEB	3.68	1.16	0.69	0.47	4.55	1.64	0.80	0.50
TFB	3.89	1.29	0.70	0.51	4.52	1.63	0.77	0.55

Table 5Probabilistic seismic demand parameters for bridge components considering PGV as *IM*

<i>EDPs</i>	<i>Models</i>							
	C_1S_1				C_3S_3			
	$\ln(a)$	b	R^2	$\beta_{D/IM}$	$\ln(a)$	b	R^2	$\beta_{D/IM}$
<i>IM</i> = PGV								
Col	-3.98	1.10	0.53	0.63	-3.32	0.89	0.58	0.46
LEB	0.12	1.07	0.58	0.56	0.82	0.87	0.56	0.46
LFB	-0.12	1.14	0.57	0.60	-1.04	1.33	0.65	0.59
TEB	-0.18	0.85	0.37	0.68	-1.51	1.36	0.52	0.80
TFB	-0.65	1.02	0.43	0.71	-1.30	1.29	0.46	0.86

**Fig. 12.** Probabilistic seismic demand models for (a) column curvature ductility demand corresponding to C_3S_3 , (b) longitudinal and transverse expansion bearings of C_3S_3

6. Results and discussion

This study focuses on the seismic fragility assessment of bridge columns and bearings, considering four various structural systems (i.e., C_1 , C_2 , C_3 , and C_4 as defined in §2) and the five skew angles (i.e., S_1 , S_2 , S_3 , S_4 , and S_5). Individual fragility curves of bridge components (columns and bearings) and fragility curves of the system are generated at four damage states: slight, moderate, extensive, and complete. A comparison is made between seismic fragility curves of the bridge at component- and system-level in the following subsections (i.e., §6.1.1 and §6.2.1). As the fragility can be investigated by evaluating the relative changes in median PGA values (Ramanathan et al. 2012; Abbasi and Moustafa 2019), a more detailed comparison between the seismic vulnerability of bridge systems based on median PGAs is presented in §6.1.2 and §6.2.2 for the component and system levels, respectively.

6.1. Component-level fragility assessment

6.1.1. Component fragility curves

To study the seismic vulnerability of columns in the various structural systems, their fragility curves are presented in Figs. 13a to d for the four damage states. More specifically, Fig. 13a displays the difference between column fragilities at the slight limit state considering different structural systems with S_1 . As it can be perceived from the figure, column vulnerability is not significantly influenced by the types of structural systems, particularly for C_3S_1 and C_4S_1 models. The curves of C_3 and C_4 intersect within the range of PGAs, making it difficult to distinguish which structural system is more susceptible to damage. However, appreciable differences can be seen between seismic fragility curves of columns at other limit states Figs. 13a to d. For instance, probability of the moderate damage to the bridge column in the C_1S_1 model is approximately 77% at $PGA = 1g$, whereas it is 18% for the C_3S_1 model (see Fig. 13b). Referring to Figs. 13a to d, the lowest likelihood of exceeding a given limit state relates to the C_3S_1 model. Besides, the fragility curves of C_1S_1 are above those of the three other models, suggesting that this model is more susceptible to damage than the other models. Similar trends associated with the column fragility have been observed for other skew angles examined in the bridge models.

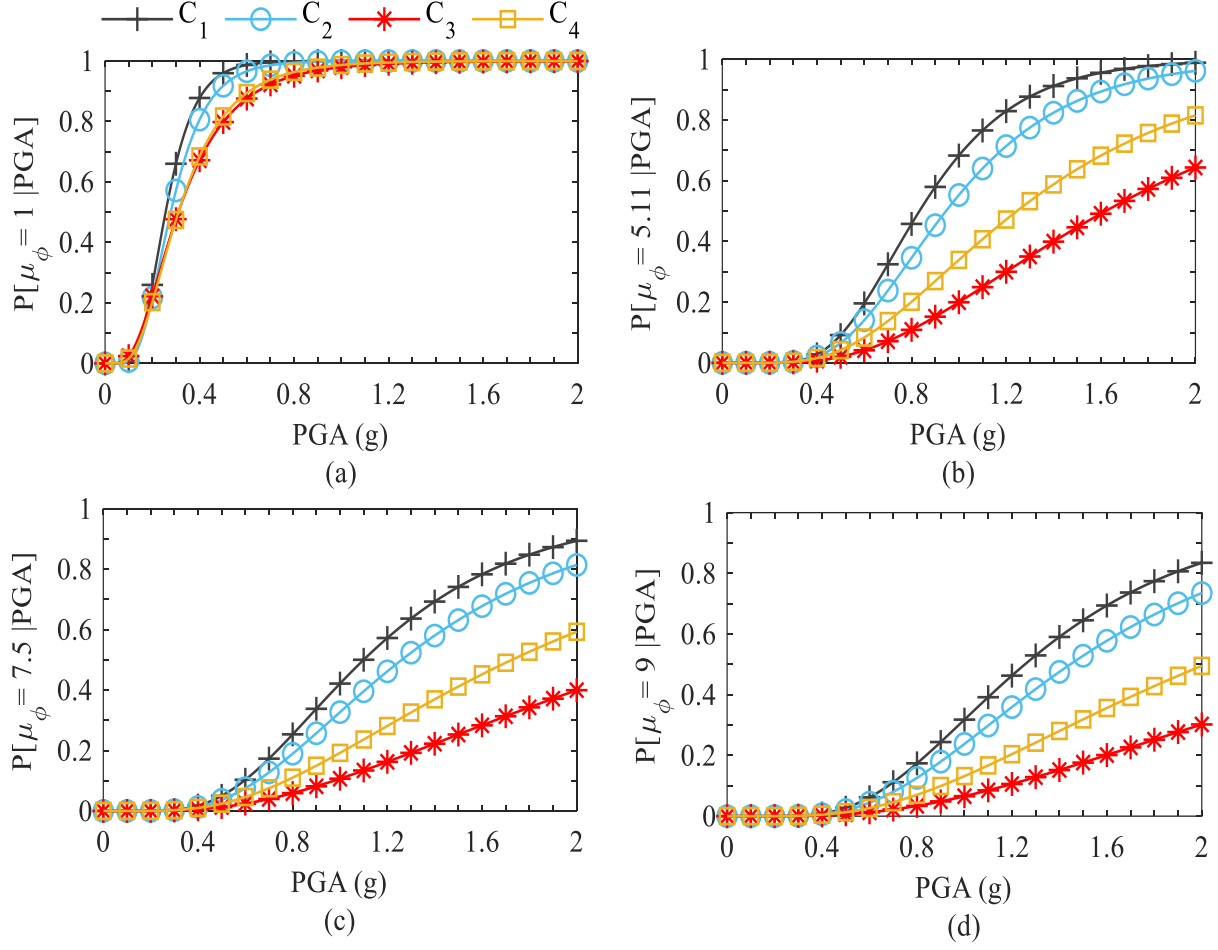


Fig. 13. Fragility curves for column curvature ductility demand considering four different structural systems with 0° skew angle at (a) slight, (b) moderate, (c) extensive, and (d) complete limit states

Figs. 14a and b illustrate a comparison fragility curves for two different types of bearings. It can be concluded from the figures that adopting various types of structural systems for bridge affects the seismic vulnerability of the bearings. The fragility curves of longitudinal expansion bearings are plotted in Fig. 14a for C_1 , C_2 , C_3 and C_4 in S_1 at the moderate limit state. This figure shows roughly identical fragilities for longitudinal expansion bearings in C_1 , C_2 , and C_4 . However, this component suggests the lowest fragility for C_3S_1 in comparison to the other structural systems. On the other hand, Fig. 14b shows that the highest probability of the moderate damage associated with the transverse fixed bearing relates to the C_3S_1 model. Furthermore, the lowest fragility of this component pertains to C_1S_1 .

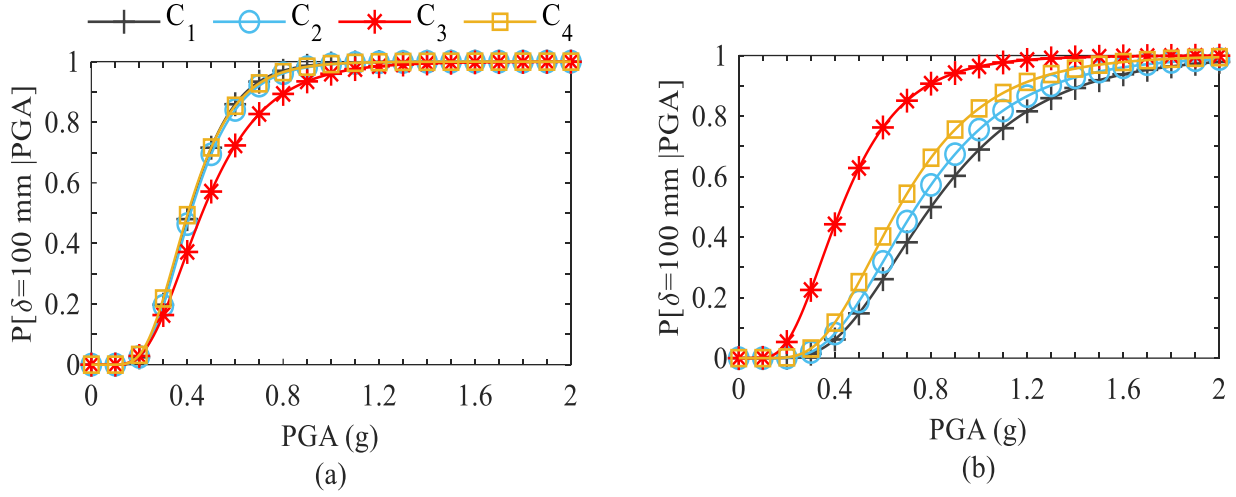


Fig. 14. Fragility curves of RC I-girder bridges under the influence of the various assumptions of structural systems for (a) longitudinal expansion bearing (LEB), (b) transverse fixed bearing (TFB) - with S_1 at the moderate damage state

The column fragility curves for skewed RC I-girder bridges are illustrated in Figs. 15a and b at the moderate limit state. Specifically, the impacts of various skew angles on the vulnerability of bridge columns assuming C_3 are addressed using fragility curves in Fig. 15a. The curves concerning the C_3S_2 and C_3S_3 models demonstrate the highest vulnerability when compared to the rest of the models. Moreover, columns in the C_3S_5 model are less susceptible to the damage than those in the other skewed models. Conversely, the columns of bridges assuming C_1 are less sensitive to variation in the skew angle. The column fragility curves of C_1 are exhibited in Fig. 15b for scenarios S_1 to S_5 . From the comparison of these fragility curves, it can be perceived that the skew angle has a minor impact on the column fragility in C_1 models.

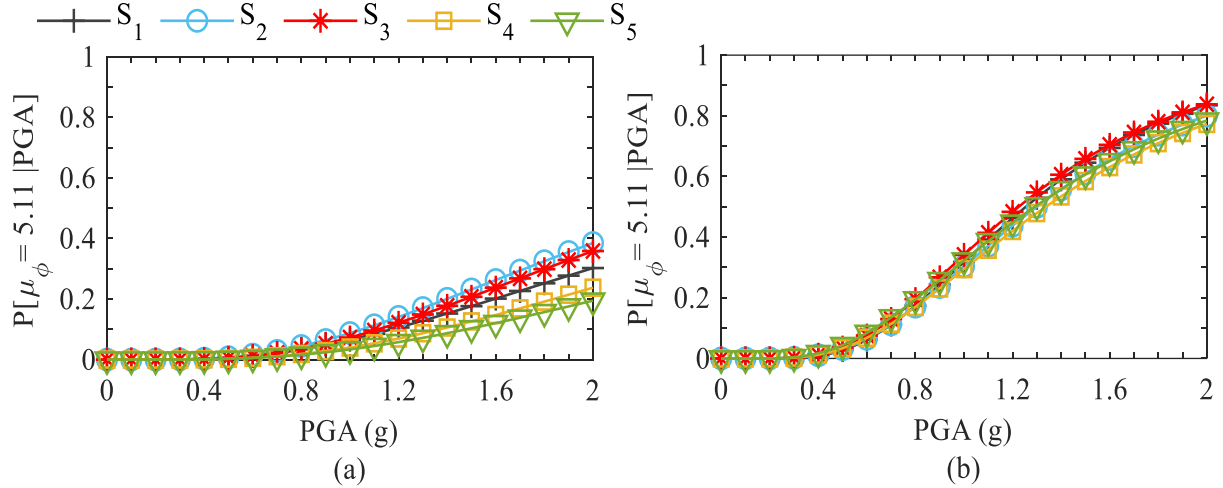


Fig. 15. Seismic fragility curves for the column curvature ductility demand across the five different skew angles at the moderate limit state for (a) C_3 , (b) C_1 - S_1 to S_5 represent skew angle from 0° to 60° in increments of 15°

Seismic fragility curves of the five bridge components defined in Table 2 are presented in Figs. 16a to d at the extensive limit state. Each plot demonstrates fragility curves of a specific structural system with S_4 . As indicated in these figures, the column is the least vulnerable component in comparison to the other components. Furthermore, in accordance with Figs. 16b and d, the fragility curves of the fixed and expansion bearings are quite similar along transverse and longitudinal directions for each model of C_2S_4 and C_4S_4 . However, referring to Figs. 16a and c, the aforementioned components in C_1S_4 and C_3S_4 indicate dissimilar probabilities of damage state exceedance. It is evident that the probability of damage for the

column in the four examined limit states in the cases of C_3 and C_4 across five skew angles is the lowest among the five components.

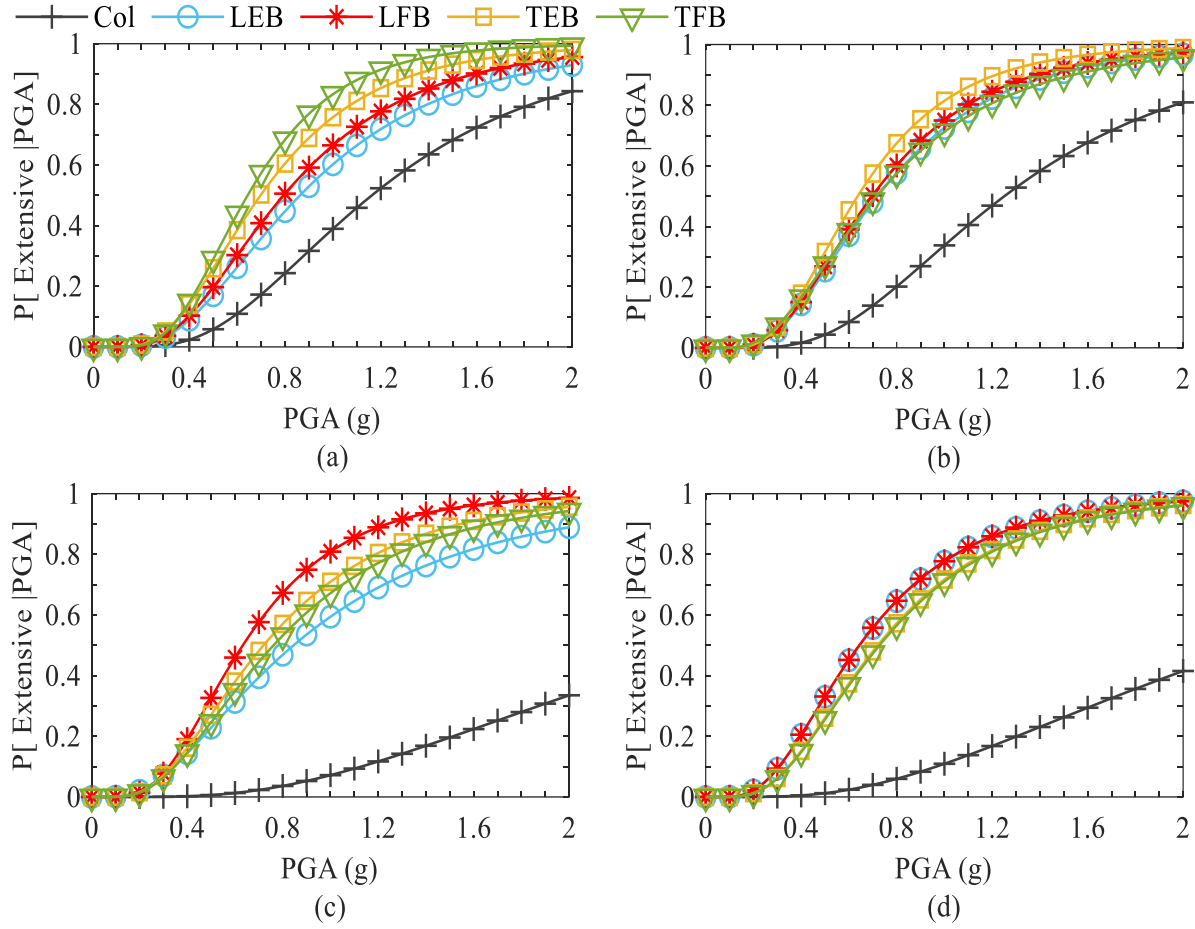


Fig. 16. Component seismic fragility curves of bridge for (a) C_1S_4 , (b) C_2S_4 , (c) C_3S_4 , and (d) C_4S_4 - at the extensive limit state

6.1.2. Component fragility medians

This is a relatively straightforward technique to compare differences in the fragility curves. A positive shift in the median PGA value indicates that the bridge components become less fragile, and vice versa. In Figs. 17a to e, the fragility medians at the extensive limit state are illustrated for different bridge components. The median PGAs for columns are depicted in Fig. 17a. The minimum of these values indicates the highest vulnerability, and the maximum of them accounts for the lowest vulnerability. The lowest fragility, concerning column curvature ductility demand, pertains to the C_3S_1 model amongst the regular bridge models. Apart from C_3S_1 , the columns of the C_4S_1 , C_2S_1 , and C_1S_1 models occupy the second through the fourth places for the lowest vulnerability. For example, the median PGAs for column curvature ductility demand are estimated 1.099g, 1.260g, 2.389g, and 1.725g for the straight bridge model assuming C_1 , C_2 , C_3 and C_4 . In fact, in the cases of C_2 , C_3 , and C_4 , the fragility of the columns decreases by 14.6%, 117.4%, and 56.9% when compared to C_1 . The same trend is generally observed for the other three limit states. As shown in Table 6, the impact of different structural systems on column vulnerability is less pronounced at the slight limit state.

Table 6

Median PGAs of the obtained fragility functions at slight damage state for bridge components

Models	Components					Models	Components				
	Col	LEB	LFB	TEB	TFB		Col	LEB	LFB	TEB	TFB
C ₁ S ₁	0.26	0.16	0.17	0.38	0.33	C ₃ S ₁	0.31	0.16	0.21	0.23	0.23
C ₁ S ₂	0.26	0.17	0.17	0.30	0.32	C ₃ S ₂	0.28	0.15	0.20	0.24	0.24
C ₁ S ₃	0.25	0.17	0.18	0.27	0.24	C ₃ S ₃	0.28	0.14	0.20	0.25	0.26
C ₁ S ₄	0.25	0.19	0.19	0.23	0.21	C ₃ S ₄	0.31	0.15	0.21	0.22	0.22
C ₁ S ₅	0.25	0.22	0.22	0.19	0.19	C ₃ S ₅	0.32	0.17	0.22	0.16	0.17
C ₂ S ₁	0.28	0.16	0.17	0.30	0.30	C ₄ S ₁	0.31	0.15	0.15	0.23	0.23
C ₂ S ₂	0.26	0.16	0.16	0.27	0.25	C ₄ S ₂	0.29	0.15	0.15	0.20	0.20
C ₂ S ₃	0.27	0.17	0.17	0.23	0.22	C ₄ S ₃	0.31	0.15	0.15	0.17	0.17
C ₂ S ₄	0.27	0.18	0.18	0.21	0.20	C ₄ S ₄	0.33	0.16	0.16	0.16	0.16
C ₂ S ₅	0.28	0.19	0.20	0.19	0.20	C ₄ S ₅	0.33	0.16	0.16	0.14	0.14

According to Fig. 17a, the median PGAs for the columns in straight bridge models of C₁ and C₂ are nearly the same. This can be justified by referring to the fact that including steel dowels in the model of elastomeric bearings increases the stiffness of this type of connection at intermediate bents of the C₂ bridges. Therefore, the column fragility of C₂ is fairly close to C₁ where the bent-to-deck connectivity is fully pinned. From another point of view, both models of C₁ and C₂ are free to rotate, but C₁ is totally fixed along translational DOFs, and C₂ is partially restricted at translational DOFs. Nevertheless, the relative change in the column median PGAs concerning the two structural systems increases when the bridge configuration is modeled with S₅ rather than S₁.

As stated in §3.1, the main difference between model of C₂ and C₄ systems is that elastomeric bearings are modeled together with steel dowels for C₂, while they are modeled alone in the case of C₄. With C₄, the columns are less susceptible to damage because the elastomeric bearings are more ‘flexible’ than the fixed/expansion bearings, and hence, they allow relative movement between the super- and substructure. In other words, the columns of C₄ experience the less curvature demand than C₂. The columns of C₂ sustain higher demand because of the more engaging between the super- and substructure resulted from the fixed/expansion bearings. Furthermore, as elaborated in §2, C₃ is constituted from separated spans, each of which is capable of moving individually. In other words, a smaller portion of deck mass is affected by seismic excitations when compared to the other structural systems. It demonstrates that the seismic demands on columns in C₂S₁ can indeed be larger than those for C₃S₁.

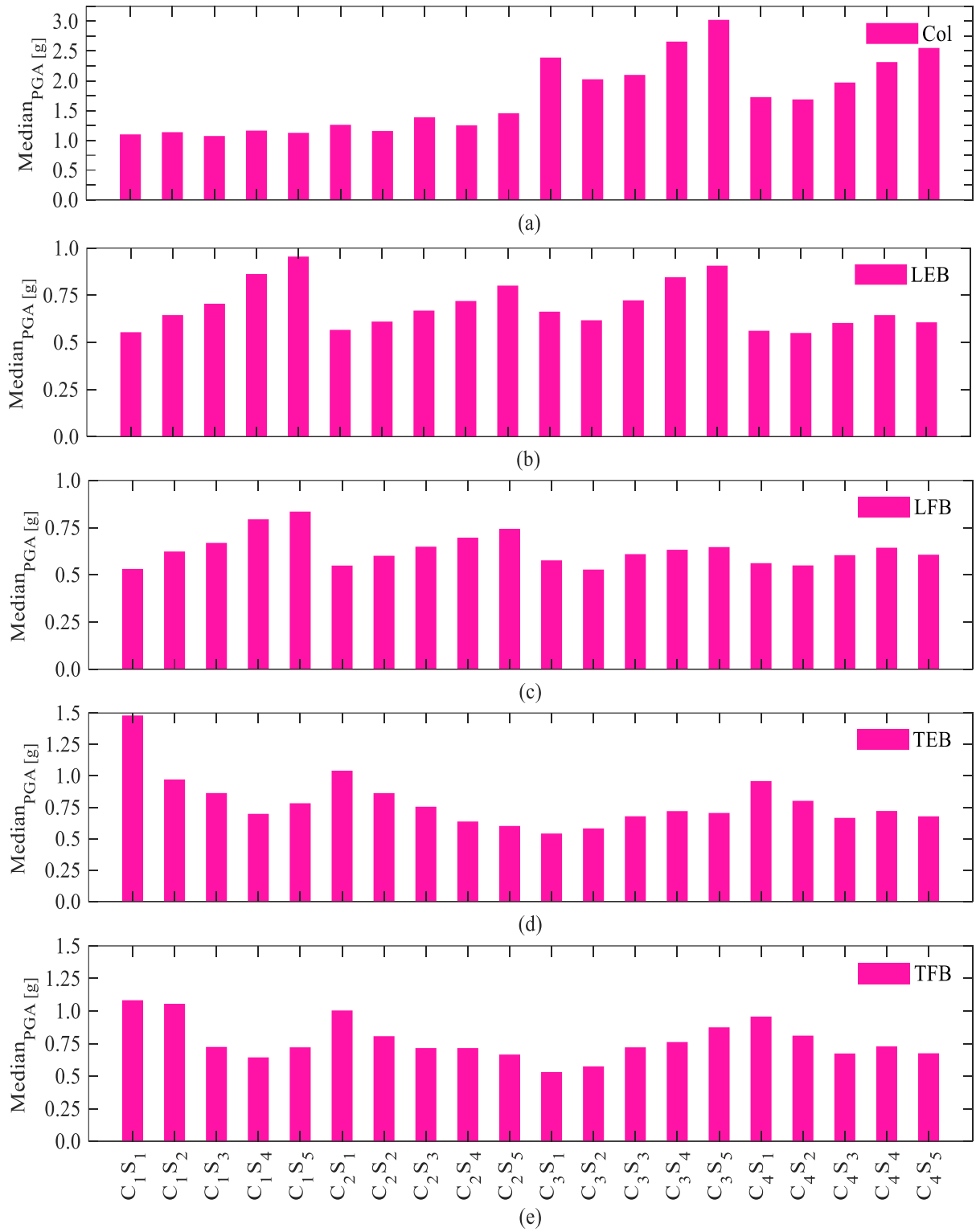


Fig. 17. Median PGAs of the obtained fragility functions for the extensive limit state corresponding to (a) column curvature ductility demand, (b) longitudinal expansion bearing, (c) longitudinal fixed bearing, (d) transverse expansion bearing, and (e) transverse fixed bearing - S_1 to S_5 represent skew angle from 0° to 60° in increments of 15°

Based on Fig. 17a, the different structural systems affect the seismic response of columns not only in bridge models with skew angle of 0° but also in models with other angles of skewness (i.e., $\theta \neq 0^\circ$). Accordingly, the order of column vulnerability from highest to lowest relates to C_1 , C_2 , C_4 , and C_3 . The column median PGAs are 1.125g, 1.453g, 2.551g, and 3.023 g for C_1S_5 , C_2S_5 , C_4S_5 , and C_3S_5 , respectively. In other words, C_2S_5 , C_4S_5 , and C_3S_5 exhibit median PGAs that are 29.1%, 126.7%, and 168.7% greater

than C_1S_5 . This attests that C_3 renders the least fragility in terms of column curvature ductility, unlike C_1 , which is the most fragile. Furthermore, considering skew angles from S_2 to S_5 , the similar trends can be found in the moderate and complete limit states as well.

In Fig. 17a, it can be observed that columns in the two structural systems, C_3 and C_4 , are sensitive to the angle of skewness. However, it is important to note that this sensitivity diminishes when adopting C_2 . The median PGAs corresponding to the curvature ductility demands of columns in C_2 , across S_1 to S_5 , are 1.260g, 1.156g, 1.386g, 1.254g, and 1.454g, respectively. On the other hand, these values for the structural system of C_3 are 2.389g, 2.025g, 2.098g, 2.653g, and 3.023g, assuming the same order of skew angles for the bridge. Nonetheless, the figure also exhibits that the lowest fluctuation in median PGAs is given by C_1 . Consequently, the bridge columns of C_1 across five levels of skewness indicate approximately equal fragility median values, unlike C_3 and C_4 , which display the most changes in the median PGAs. These trends can also be found at the moderate and complete limit states.

Among all the bridge models investigated in Fig. 17a, the minimum median PGA 1.072g is given by the C_1S_3 model, whereas this occurs in other structural systems with S_2 , e.g., C_2S_2 . Similar results are also observed for the other limit states. Meanwhile, it can be generally resulted, with trivial exceptions such as C_3S_2 , that as the angle of skewness is increased, the median PGAs of columns increase, indicating the beneficial role of skewness, especially beyond S_3 for C_3 and C_4 models. In other words, the greater angle of skewness results in the lower vulnerability of columns. To sum up, by increasing skewness, particularly beyond a medium level of angle, the fragility of columns in the cases of C_3 and C_4 diminishes for all the four limit states.

The median PGAs are presented in Figs. 17b to e, corresponding to the extensive damage on the expansion and fixed bearings along longitudinal and transverse directions of the bridge models. It should be noted that the seismic response of bearings is examined at abutments only in the case of the C_1 model, as bent-to-deck connectivity is pinned. Based on Fig. 17b, the median PGAs for the longitudinal expansion bearing of the straight model vary from 0.553g for C_1 to 0.566g, 0.662g, and 0.561g for C_2 , C_3 , and C_4 , respectively. This indicates that the vulnerability of the longitudinal expansion bearing varies depending on the type of structural system. Additionally, these values for the same component in S_5 are 0.955g, 0.801g, 0.906g, and 0.606g, revealing the sensitivity of the longitudinal expansion bearing to the skewness. According to Fig. 17c, the longitudinal fixed bearings are also sensitive to the assumptions associated with the structural systems and skewness. Furthermore, a similar conclusion can be drawn at the other limit states. In addition, Figs. 17b and c illustrate that the longitudinal expansion bearing exhibits lower vulnerability compared to the fixed bearing in the same direction for C_1 , C_2 , and C_3 .

Referring to Figs. 17b and c, despite some exceptions, such as longitudinal bearings of the C_3S_2 model, which fragility peaks out among the other angles, generally, as the skew angle increases, the bearings become less fragile. For example, with reference to Fig. 17c, the fragility medians 0.548g, 0.600g, 0.649g, 0.698g, and 0.743g related to the longitudinal fixed bearing are obtained for C_2S_1 , C_2S_2 , C_2S_3 , C_2S_4 , and C_2S_5 . It means that by changing the bridge configuration from S_1 to S_5 , the probability of attaining the extensive damage to the longitudinal fixed bearings is reduced by 35%. In total, increasing skew angle contributes to the reduction of the fragility of the longitudinal bearings for models with C_1 , C_2 , C_3 , and C_4 .

In the cases of C_1 , C_2 , and C_4 , transverse bearing fragility increases as skew angle increases, in contrast to the other types of bearings. For example, the median PGAs for the transverse expansion bearings of the bridge model with C_2 corresponding to S_1 through S_5 are 1.041g, 0.862g, 0.754g, 0.636g, and 0.601g, respectively. However, when C_3 is included in modeling, the fragility of the transverse bearings decreases as the skewness increases. Referring to Fig. 17d, median PGAs 0.541g, 0.581g, 0.678g, 0.719g, and 0.704g are associated with the transverse expansion bearings of the C_3 models from S_1 to S_5 , respectively. It means that by switching from C_3S_2 to C_3S_3 , a 16.6% reduction in the seismic fragility is achieved. Additionally, these trends concerning the transverse bearings hold true at the moderate and complete limit states for all the structural systems.

It is evident from Figs. 17b to e that the presence of steel dowel inside the fixed and expansion bearings is a contributing factor in reducing the vulnerability of the bearings. For example, in the case of C_2S_5 , the vulnerability of longitudinal expansion bearings is 32.1% lower than that of longitudinal bearings

of the C_4S_5 model. Overall, the longitudinal bearings with C_4 are generally more fragile than those of C_2 . The trend is consistent across all the damage states.

To compare the seismic vulnerability of the column with that of bearings, their median PGAs corresponding to the moderate limit state are plotted in Figs. 18a to d for each structural system versus different skew angles. According to Figs. 18c and d, the bearings are more vulnerable than the columns. It should be noted that the bridge columns of C_3 and C_4 are considerably less vulnerable than the transverse or longitudinal bearings for all the angles of skewness. These results can also be observed at the other limit states. For instance, the fragility medians of the column in C_3 are equal to 1.62g, 1.39g, 1.43g, 1.77g, and 1.97g for S_1 to S_5 , respectively. The corresponding values for the longitudinal expansion bearing in the same structural system are 0.46g, 0.43g, 0.48g, 0.54g, and 0.59g for S_1 to S_5 . This means that the seismic vulnerability of the columns for the five skew angles is by 252.1%, 202.2%, 297.9%, 221.8%, and 228.3% lower compared to that of the longitudinal expansion bearings. Similarly, the vulnerability of the transverse expansion bearings in the C_3 models from S_1 to S_5 is 3.77, 3.02, 2.7, 3.34, and 5.1 times that of the column, respectively. Altogether, the lowest vulnerability at the four limit states and amongst all the components is given by bridge columns assuming C_3 and C_4 .

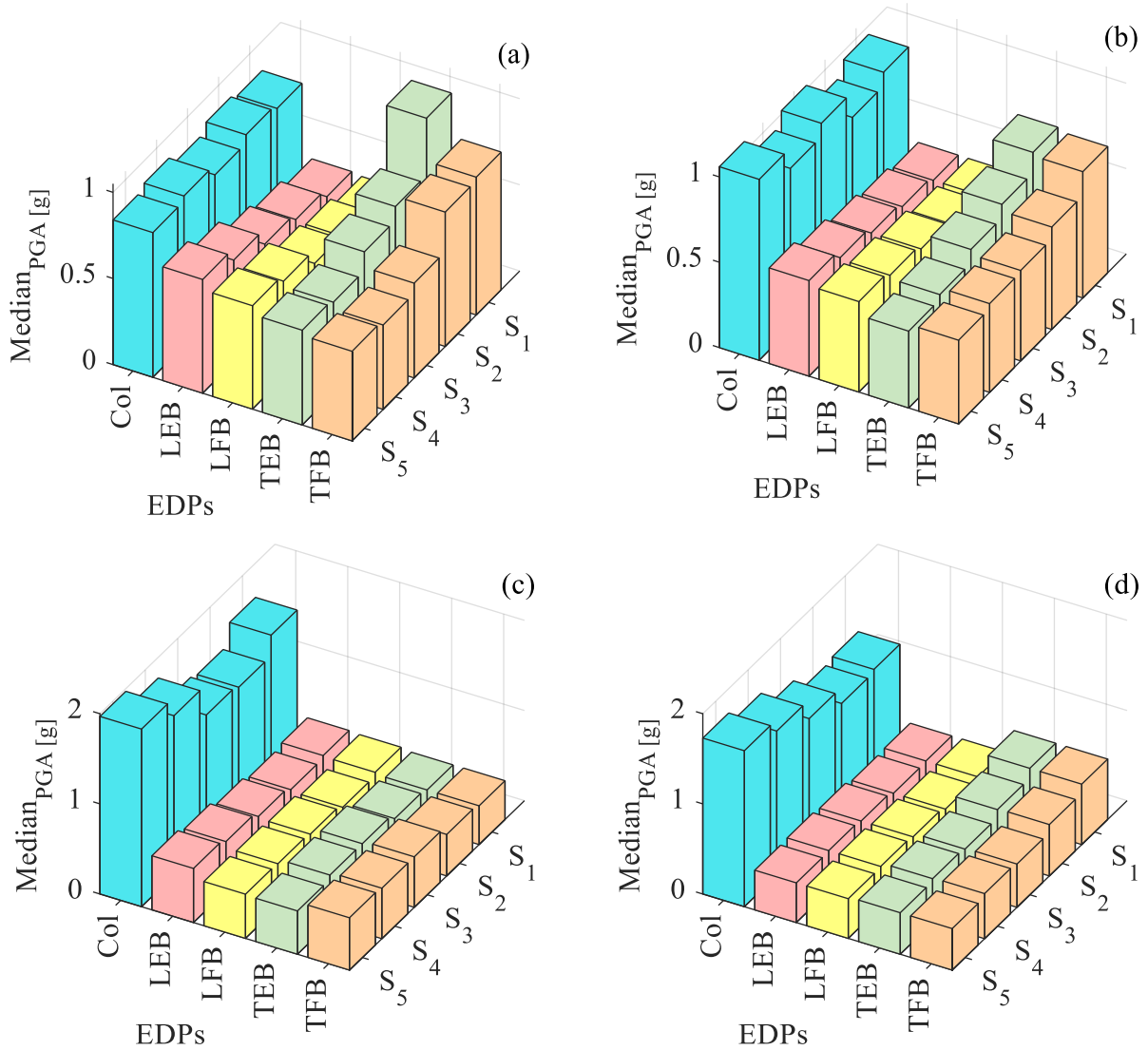


Fig. 18. Median PGAs of the obtained fragility functions at the moderate damage state for different bridge components assuming various structural systems: (a) C_1 , (b) C_2 , (c) C_3 , and (d) C_4 versus skew angles - S_1 to S_5 represent skew angle from 0° to 60° in increments of 15°

6.1.3. Fragility median ratios of column curvature ductility

The ratio defined in Eq. (5) is used to comprehend the simultaneous effects of structural systems and skew angles on the seismic fragility of columns across the four limit states. The equation is as follows:

$$R = \frac{\text{median}(C_m S_n)}{\text{median}(C_1 S_n)} \quad (5)$$

where R is the median PGA of a bridge column obtained for the m^{th} structural system (C_m) divided by that obtained for the model with pinned connection (C_1) at the n^{th} skew angle (S_n).

Figs. 19a to d illustrate the R ratios for the various models across the four limit states. As evident from comparing the R ratios, columns are strongly influenced by different structural systems at some angles of skewness, e.g., C_2S_4 and C_4S_4 (see Fig. 19a). However, for certain angles, the figure shows that the impacts of different structural systems on column are inconsequential. As a result, the noticeable effects of structural systems on the regular bridge columns may be largely alleviated when considering skewness.

As plotted in Figs. 19a to d, the R ratios corresponding to C_3 and C_4 are roughly equal for certain angles. In accordance with Fig. 19c, the R ratios of 1.95 and 1.83 pertain to the C_3S_3 and C_4S_3 models. Besides, the R ratios for C_1S_2 and C_2S_2 are approximately identical for the three limit states of slight, moderate, and extensive. Although the relative change in the R ratios between C_2 and C_4 are significant at most cases (e.g., 0.76 for S_4 at the moderate limit state), this value is 0.22 in case of S_5 at the complete damage state. Consequently, a skewed superstructure at certain angles for various limit states may significantly reduce the response sensitivity of columns to the variations of the structural systems.

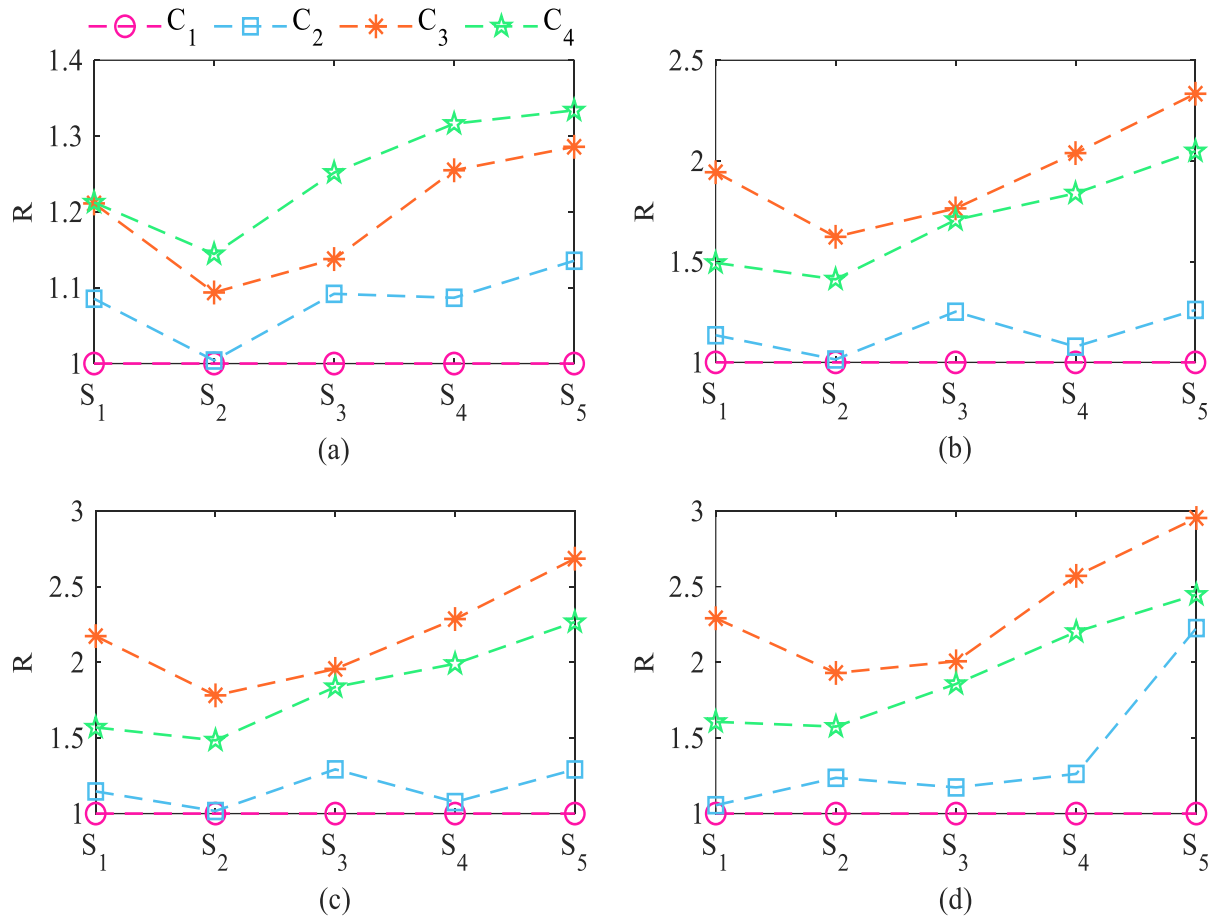


Fig. 19. R values for different skew angles at (a) slight, (b) moderate, (c) extensive, and (d) complete limit states

6.2. System-level fragility assessment

6.2.1. System fragility curves

For the regular bridge ($\theta = 0^\circ$, S_1), the system fragility curves corresponding to the four structural systems examined in this study are presented in Figs. 20a to d for slight, moderate, extensive, and complete damage states. Comparison of the bridge system fragilities reveals that structural systems C_3 and C_4 exhibit the highest and lowest vulnerability across all damage states. It is observed that the structural systems C_1 and C_2 exhibit similar vulnerability. For instance, at $\text{PGA} = 1\text{g}$, the probability of complete damage reaches 81% for the C_3S_1 model, compared to 58% for C_4S_1 (Fig. 11d). In contrast, C_1S_1 and C_2S_1 exhibit nearly identical fragility, with probabilities of 65% and 64%. To summarize, for the regular bridges across all limit states, C_4 exhibits the lowest probability of exceedance, whereas C_3S_1 demonstrates the highest vulnerability. In contrast, C_1 and C_2 demonstrate comparable vulnerability.

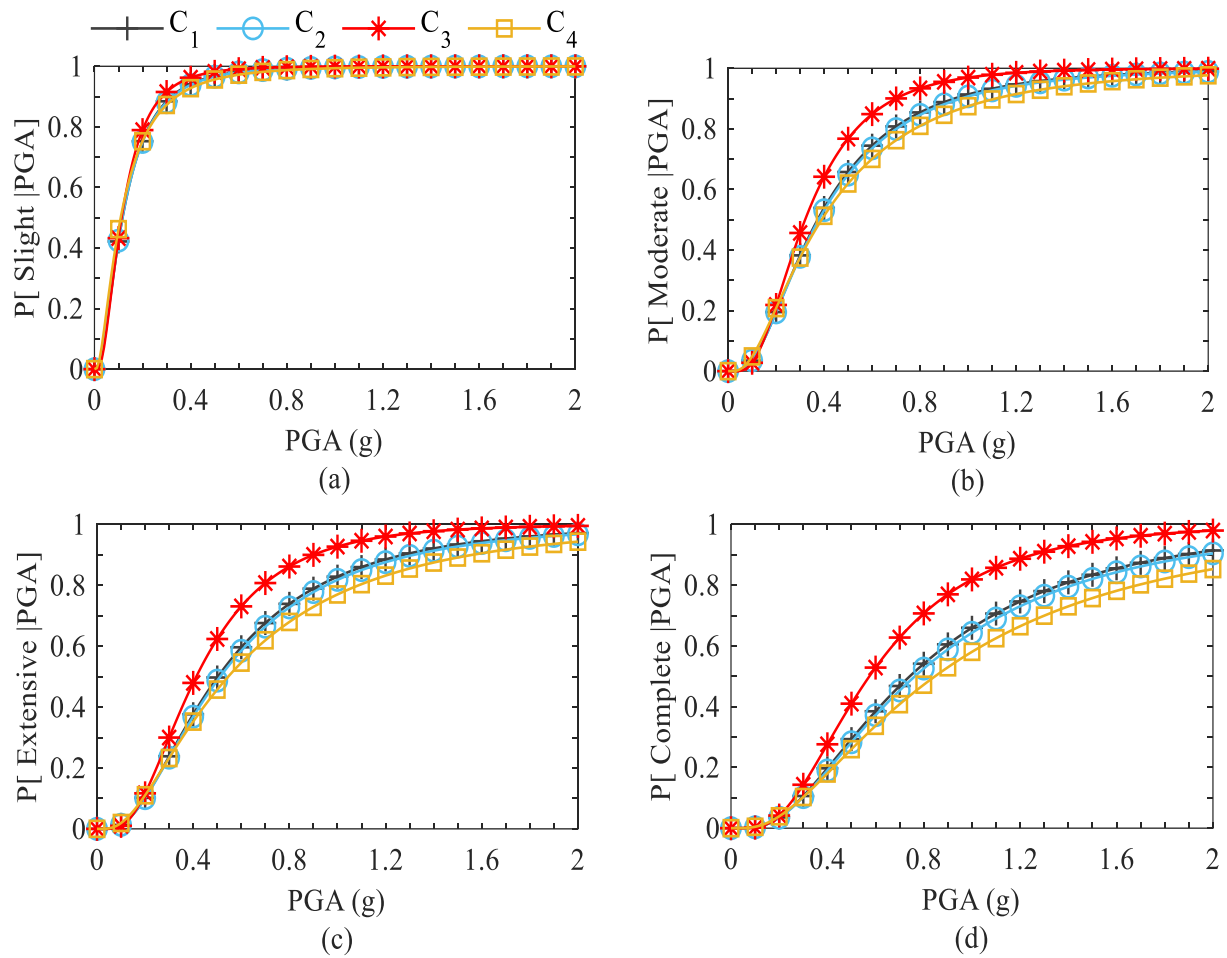


Fig. 20. System fragility curves of RC I-girder bridges under the influence of the various assumptions of structural systems with S_1 at (a) slight, (b) moderate, (c) extensive, and (d) complete limit states

Figs. 21a and d present the bridge system fragility curves across five skew angles (S_1 to S_5 , corresponding to skew angles 0° to 60°) at the extensive damage limit state. Fig. 21a specifically examines the influence of skew angle on the vulnerability of C_3 structural system. The results reveal that system fragility in C_3 structural system is sensitive to variation in skew angles. In contrast, Fig. 21b illustrates the bridge fragility curves for C_4 , showing minimal sensitivity to skew angle changes. Findings indicate that the fragility of both C_2 and C_4 is insensitive to skew angle variations, while C_1 and C_3 demonstrate sensitivity across all limit states. The remainder of this section presents and discusses the fragility median values for the bridge system.

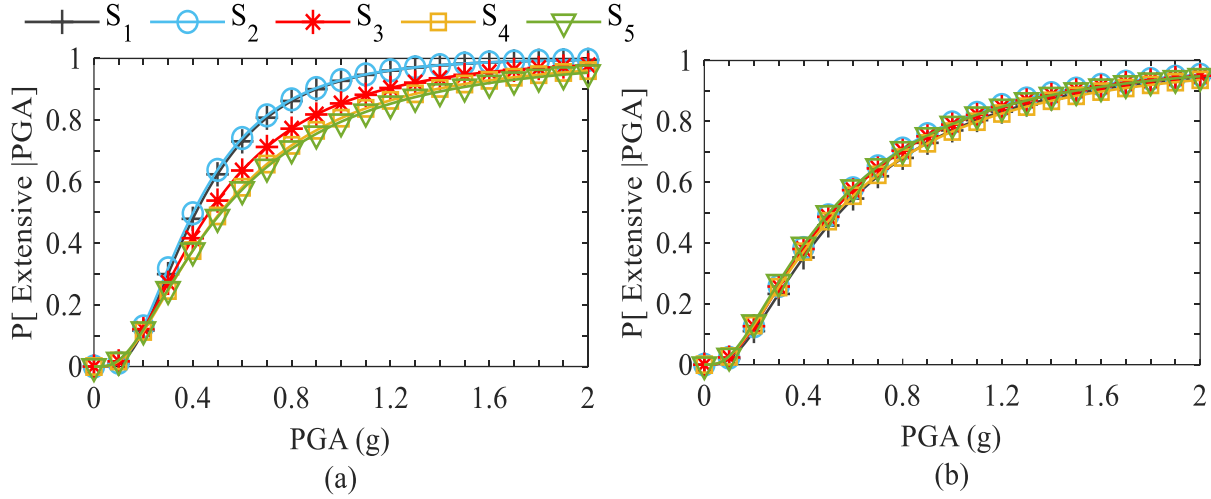


Fig. 21. System fragility curves for (a) C_3 , (b) C_4 across the five different skew angles at the extensive limit state - S_1 to S_5 represent skew angle from 0° to 60° in increments of 15°

6.2.2. System fragility medians

The parameters of the system fragility functions, i.e., median (S) and dispersion (β), for all bridge models are summarized in Table 6. The table indicates similar median PGAs for all bridge models at the slight damage state. However, at more severe damage states (extensive and complete), greater variation emerges in the system's fragility medians.

Table 7

Median and dispersion values for bridge system fragility

Model	S_s^*	β_s	S_m	β_m	S_e	β_e	S_c	β_c
C_1S_1	0.117	0.787	0.373	0.724	0.503	0.725	0.742	0.725
C_1S_2	0.118	0.862	0.418	0.796	0.581	0.798	0.885	0.795
C_1S_3	0.122	0.819	0.409	0.753	0.560	0.755	0.834	0.754
C_1S_4	0.122	0.800	0.398	0.733	0.540	0.733	0.796	0.731
C_1S_5	0.112	0.892	0.423	0.821	0.597	0.822	0.914	0.812
C_2S_1	0.117	0.800	0.377	0.736	0.512	0.737	0.763	0.736
C_2S_2	0.113	0.820	0.378	0.764	0.521	0.767	0.791	0.767
C_2S_3	0.111	0.810	0.369	0.748	0.507	0.750	0.767	0.753
C_2S_4	0.113	0.792	0.366	0.732	0.498	0.732	0.746	0.732
C_2S_5	0.112	0.804	0.367	0.738	0.500	0.739	0.750	0.739
C_3S_1	0.113	0.712	0.321	0.608	0.413	0.608	0.574	0.608
C_3S_2	0.108	0.715	0.310	0.618	0.402	0.620	0.564	0.622
C_3S_3	0.112	0.776	0.344	0.723	0.466	0.725	0.692	0.727
C_3S_4	0.111	0.844	0.370	0.778	0.511	0.778	0.778	0.778
C_3S_5	0.106	0.878	0.369	0.807	0.516	0.805	0.797	0.803
C_4S_1	0.109	0.892	0.390	0.820	0.546	0.819	0.847	0.819
C_4S_2	0.102	0.880	0.363	0.813	0.509	0.814	0.792	0.814
C_4S_3	0.101	0.892	0.365	0.826	0.515	0.826	0.807	0.827
C_4S_4	0.096	0.936	0.370	0.867	0.532	0.868	0.857	0.869
C_4S_5	0.095	0.913	0.353	0.848	0.503	0.848	0.800	0.849

* The subscripts s , m , e , c denote slight, moderate, extensive and complete damage states.

To facilitate direct comparison, Figs. 22a and b display the system fragility medians corresponding to the extensive and complete damage states. In Figs. 22a and b, the highest and lowest bridge system fragility pertains to C_3 and C_4 assuming the regular bridge model S_1 . The system fragilities of C_1S_1 and C_2S_1

are comparable, falling between the fragility levels of the aforementioned structural systems. For example, the median PGAs for the system fragility at the complete damage state are estimated 0.57g, 0.74g, 0.76g, and 0.84g for the straight bridge model assuming C_3 , C_1 , C_2 and C_4 , respectively. Quantitative comparisons also indicate that C_3 is more vulnerable at S_1 to S_3 , compared to alternative systems. In contrast, C_2 shows higher seismic vulnerability at higher skew angles (S_4 and S_5).

As shown in Figs. 22a and b, the influence of skew angle variations on bridge system vulnerability is relatively minor for C_2 and C_4 structural systems at the extensive and complete limit states. Based on the figures, the structural system C_2 is insensitive to variation in skew angles at the extensive damage state, with median fragility values confined to a narrow band between 0.498g (S_4) and 0.521g (S_2), varying by less than 5% across all skew angles. However, the system fragility medians of C_1 and C_3 show significantly greater sensitivity to skewness effects at the extensive and complete limit states. At the complete limit state, the median PGAs for bridge system increase with higher skew angles, exhibiting a 41% variation across the examined range of skew angles (0° to 60°). The study concludes that while bridge skewness can influence the performance of C_1 and C_3 structural systems in the bridge models, its effect on C_2 and C_4 is negligible.

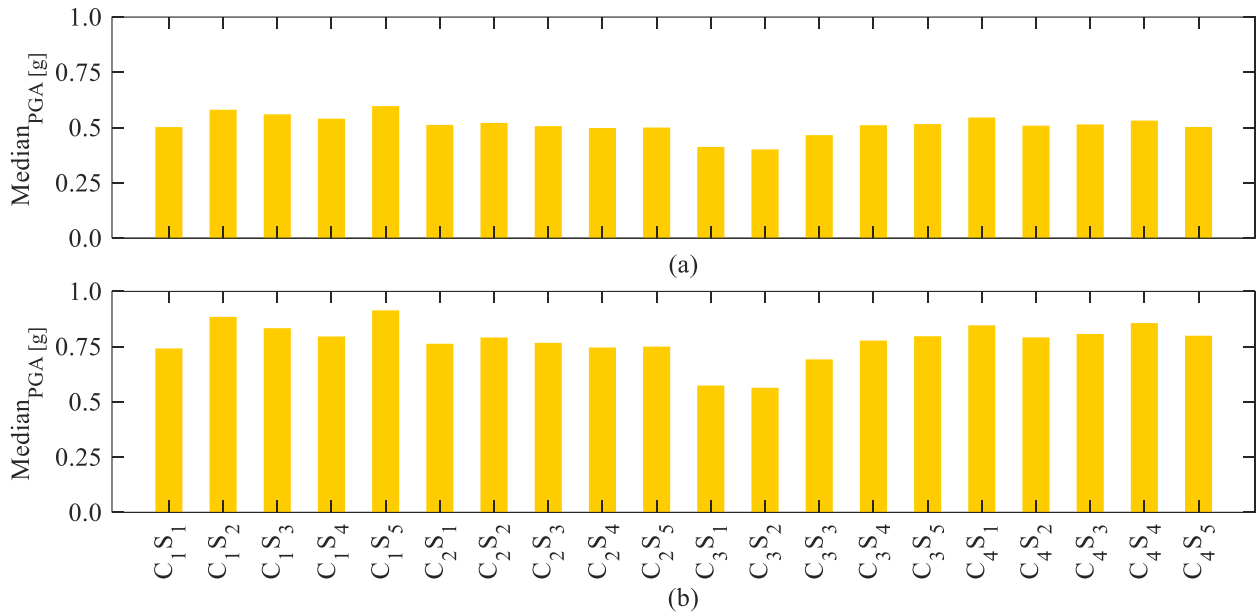


Fig. 22. Median PGAs of the obtained system fragility functions across all the bridge models at (a) extensive, (b) complete limit states - S_1 to S_5 represent skew angle from 0° to 60° in increments of 15°

7. Conclusion

This study aims to examine the combined effects of various structural systems and skewness on the seismic behavior of seismically-designed multi-span reinforced concrete I-girder bridges. In this respect, the two most common structural systems including multi-span simply supported (C_3) and multi-span continuous girders are considered. The latter structural system in this study is categorized using three different assumptions in terms of boundary conditions including continuous girders with pinned bent-to-deck connectivity (C_1), continuous girders resting on elastomeric bearings along with steel dowels (C_2), and continuous girders resting on elastomeric bearing without steel dowels (C_4).

The results proved that bridge fragility characteristics vary depending on the type of structural system or skew angle under consideration. It is seen that the response sensitivity of the column to the variation of the structural systems may considerably decrease when implementing skewed superstructure. The relative change in fragility medians of the column corresponding to C_3 and C_4 structural systems in the skewed bridges (skew angle of 30°) is about 6 times less than that of the straight bridges (skew angle of 0°). The seismic vulnerability of the column is significantly more pronounced under the effects of skew angles in bridges with the C_3 and C_4 structural systems in comparison to bridges assuming C_1 and C_2 . Besides, the skewness plays a beneficial role in reducing the column vulnerability of bridges modeled using C_3 and C_4

structural systems such that, in most cases, the column vulnerability diminishes as the skew angle rises. Given the deployment of different structural systems in the bridges, the order of the column vulnerability from highest to lowest pertains to C_1 , C_2 , C_4 , and C_3 . It is also noted that the vulnerability of longitudinal fixed and expansion bearings decreases with increasing skew angles. However, the skewness has an adverse impact on the fragility of transverse fixed and expansion bearings in the bridges with C_1 , C_2 , and C_4 structural systems. Interestingly, for bridges assuming C_3 , as the skew angle increases, the fragility of transverse bearings is actually reduced.

Structural system C_3 exhibit greater system-level vulnerability at lower skew angles (0° to 30°) compared to the other structural systems. In contrast, C_2 is the most vulnerable at higher skew angles. The study concludes that while variation in skew angles can influence the seismic vulnerability of C_1 and C_3 structural systems, its effects on the vulnerability of C_2 and C_4 is negligible.

The findings of this paper highlight that both structural system and skewness angle of bridges can have important implications for post-earthquake recovery, maintenance requirements, and lifecycle performance. Bridges with higher fragility, particularly in key components like columns and bearings, are likely to experience longer downtimes, higher repair costs, and greater disruption to transportation networks. Thus, selecting structural systems with lower fragility (e.g., C_3 in certain skew angles) can contribute to more resilient infrastructure with reduced recovery times and improved service continuity after seismic events. Future research opportunities include the need to determine the extent to which adopting various self-centering dampers as a retrofit measure can affect the seismic behavior of skewed bridges adopting the different structural systems.

References

- Abbasi M, Moustafa MA (2019) Probabilistic seismic assessment of as-built and retrofitted old and newly designed skewed multi-frame bridges. *Soil Dyn Earthq Eng* 119:170–186. <https://doi.org/10.1016/j.soildyn.2019.01.013>
- Abbasi M, Moustafa MA (2017) Effect of Shear Keys on Seismic Response of Irregular Bridge Configurations;
- Abbiati G, Cazzador E, Alessandri S, et al (2018) Experimental characterization and component-based modeling of deck-to-pier connections for composite bridges. *J Constr Steel Res* 150:31–50. <https://doi.org/10.1016/j.jcsr.2018.08.005>
- Abdelnaby AE, Frankie TM, Elnashai AS, et al (2014) Numerical and hybrid analysis of a curved bridge and methods of numerical model calibration. *Eng Struct* 70:234–245. <https://doi.org/10.1016/j.engstruct.2014.04.009>
- Aldea S, Bazaez R, Astroza R, Hernandez F (2021) Seismic fragility assessment of Chilean skewed highway bridges. *Eng Struct*. <https://doi.org/https://doi.org/10.1016/j.engstruct.2021.113300>
- Baker JW, Cornell CA (2006) Which spectral acceleration are you using? *Earthq Spectra* 22:293–312. <https://doi.org/10.1193/1.2191540>
- Baker JW, Shahi SK (2011) New Ground Motion Selection Procedures and. *Risk Manag*
- Bhaskar Panchireddi SS, Ghosh J (2023) Influence of ground motion duration on the seismic vulnerability of aging highway bridges. *Struct Infrastruct Eng* 19:1041–1063. <https://doi.org/10.1080/15732479.2021.1998141>
- Caltrans (2019) Caltrans seismic design criteria version 2.0. Sacramento, California: California Department of Transportation;
- Choi E (2002) Seismic fragility of typical bridges in moderate seismic zones. Atlanta, GA: Georgia Institute of Technology;
- Cornell CA, Jalayer F, Hamburger RO, Foutch DA (2002) Management Agency Steel Moment Frame Guidelines. *J Struct Eng* 128:526–533
- De Matteis G, Caprili S, Carbonari S, et al (2022) Critical issues in safety assessment of existing reinforced concrete bridges by means of nonlinear analysis. *Procedia Struct Integr* 44:681–688. <https://doi.org/10.1016/j.prostr.2023.01.089>
- Ellingwood BR, Wen YK (2005) Risk-benefit-based design decisions for low-probability/high consequence

- earthquake events in Mid-America. *Prog Struct Eng Mater* 7:56–70. <https://doi.org/10.1002/pse.191>
- Elnashai AS, Gencturk B, Kwon OS, et al (2012) The Maule (Chile) earthquake of February 27, 2010: Development of hazard, site specific ground motions and back-analysis of structures. *Soil Dyn Earthq Eng* 42:229–245. <https://doi.org/10.1016/j.soildyn.2012.06.010>
- Engen M, Hendriks MAN, Köhler J, et al (2017) A quantification of the modelling uncertainty of non-linear finite element analyses of large concrete structures. *Struct Saf* 64:1–8. <https://doi.org/10.1016/j.strusafe.2016.08.003>
- FEMA (2003) HAZUS-MH MR1: technical manual. Federal Emergency Management Agency, Washington (DC)
- Ghosh J (2021) Next Generation Fragility Functions for Seismically Designed Highway Bridges in Moderate Seismic Zones. 22:1–19. [https://doi.org/10.1061/\(ASCE\)NH.1527-6996.0000426](https://doi.org/10.1061/(ASCE)NH.1527-6996.0000426)
- Giovenale P, Cornell CA, Esteva L (2004) Comparing the adequacy of alternative ground motion intensity measures for the estimation of structural responses. *Earthq Eng Struct Dyn* 33:951–979. <https://doi.org/10.1002/eqe.386>
- Hou G, Asce SM, Chen S, Asce M (2017) Bent Connection Options for Curved and Skewed SMC Bridges in Low-to-Moderate Seismic Regions. 22:1–11. [https://doi.org/10.1061/\(ASCE\)SC.1943-5576.0000331](https://doi.org/10.1061/(ASCE)SC.1943-5576.0000331)
- Howard Hwang B, Jernigan JB, Lin Y-W (2000) Evaluation of seismic damage to Memphis bridges and highway systems. *J Bridg Eng* 5(4):322–30
- Huo Y, Zhang J (2013) Effects of Pounding and Skewness on Seismic Responses of Typical Multispan Highway Bridges Using the Fragility Function Method. *J Bridg Eng* 18:499–515. [https://doi.org/10.1061/\(asce\)be.1943-5592.0000414](https://doi.org/10.1061/(asce)be.1943-5592.0000414)
- Ishac MG, Mehanny SSF (2016) Do mixed pier-to-deck connections alleviate irregularity of seismic response of bridges with unequal height piers ? *Bull Earthq Eng*. <https://doi.org/10.1007/s10518-016-9958-8>
- Jankowski R (2015) Pounding between Superstructure Segments in Multi-Supported Elevated Bridge with Three-Span Continuous Deck under 3D Non-Uniform Earthquake Excitation. *J Earthq Tsunami* 9:1–18. <https://doi.org/10.1142/S1793431115500128>
- Johnson N, Ranf RT, Saïdi MS, et al (2006) Shake-table studies of a two-span, reinforced concrete bridge. 8th US Natl Conf Earthq Eng 2006 6:3615–3625. [https://doi.org/10.1061/\(asce\)st.1943-541x.0000790](https://doi.org/10.1061/(asce)st.1943-541x.0000790)
- Kabir MR, Billah AHMM, Alam MS (2019) Seismic fragility assessment of a multi-span RC bridge in Bangladesh considering near-fault, far-field and long duration ground motions. *Structures* 19:333–348. <https://doi.org/10.1016/j.istruc.2019.01.021>
- Kaviani P, Zareian F, Taciroglu E (2012) Seismic behavior of reinforced concrete bridges with skew-angled seat-type abutments. *Eng Struct* 45:137–150. <https://doi.org/10.1016/j.engstruct.2012.06.013>
- Maleki S (2005) Seismic Modeling of Skewed Bridges with Elastomeric Bearings and Side Retainers. *J Bridg Eng* 10:442–449. [https://doi.org/10.1061/\(asce\)1084-0702\(2005\)10:4\(442\)](https://doi.org/10.1061/(asce)1084-0702(2005)10:4(442))
- Mander J, Priestley M PR (1988) Theoretical stress-strain model for confined concrete. *J Struct Eng* 114:1804–1826
- Mangalathu S, Jeon J-S, Jiang J (2019) Skew Adjustment Factors for Fragilities of California Box-Girder Bridges Subjected to near-Fault and Far-Field Ground Motions. *J Bridg Eng* 24:04018109. [https://doi.org/10.1061/\(asce\)be.1943-5592.0001338](https://doi.org/10.1061/(asce)be.1943-5592.0001338)
- McKenna F (2011) OpenSees: a framework for earthquake engineering simulation. *Comput Sci Eng* 13(4):58–66
- Miner LR (2014) Effect of abutment skew and horizontally curved alignment on bridge reaction forces
- Mirzai NM, Eslamnia H, Bakhshinezhad S, Jeong S-H (2023) Seismic fragility assessment of a multi-span continuous I-girder bridge controlled by a self-centering damper. *Structures* 50:1838–1856. <https://doi.org/https://doi.org/10.1016/j.istruc.2023.02.091>
- Muthukumar S, DesRoches R (2006) A Hertz contact model with non-linear damping for pounding simulation. *Earthq Eng Struct Dyn* 35:811–828. <https://doi.org/10.1002/eqe.557>
- Nielson BG (2005) Analytical fragility curves for highway bridges in moderate seismic zones [Ph.D. thesis]. Georgia Institute of Technology
- Noori HR, Memarpour MM, Yakhchalian M, Soltanieh S (2019) Effects of ground motion directionality on seismic behavior of skewed bridges considering SSI. *Soil Dyn Earthq Eng* 127:105820.

<https://doi.org/10.1016/j.soildyn.2019.105820>

- Omranian E, Abdelnaby AE, Abdollahzadeh G (2018) Seismic vulnerability assessment of RC skew bridges subjected to mainshock-aftershock sequences. *Soil Dyn Earthq Eng* 114:186–197.
<https://doi.org/10.1016/j.soildyn.2018.07.007>
- Padgett, Jamie E. and RD (2008) Methodology for the development of analytical fragility curves for retrofitted bridges. *Earthq Engng Struct Dyn*
- Priestley MJN, Seible F CG (1996) *Seismic design and retrofit of bridges*. Hoboken, NJ, USA: John Wiley & Sons, Inc;
- Ramanathan K, Desroches R, Padgett JE (2012) A comparison of pre- and post-seismic design considerations in moderate seismic zones through the fragility assessment of multispan bridge classes. *Eng Struct* 45:559–573.
<https://doi.org/10.1016/j.engstruct.2012.07.004>
- Ramanathan KN (2012) Next generation seismic fragility curves for California bridges incorporating the evolution in seismic design philosophy. Atlanta, GA: Georgia Institute of Technology;
- Rezaei H, Mohammadi Dehcheshmeh E, Tsompanakis Y (2025) Impact of analysis method on the fragility curves of regular and irregular box-girder highway bridges. *Struct Infrastruct Eng* 0:1–21.
<https://doi.org/10.1080/15732479.2025.2491836>
- Shamsabadi A, Rollins KM (2014) Three-dimensional nonlinear continuum seismic soil-structure interaction analysis of skewed bridge abutments. *Numer Methods Geotech Eng - Proc 8th Eur Conf Numer Methods Geotech Eng NUMGE 2014* 2:933–938. <https://doi.org/10.1201/b17017-166>
- Shekhar S, Ghosh J, Ghosh S (2022) Influence of Bearing Types and Design Code Advances on Seismic Vulnerability of Simply Supported Highway Bridges. *J Earthq Eng* 26:4977–5003.
<https://doi.org/10.1080/13632469.2020.1852138>
- Soleimani F, Vidakovic B, DesRoches R, Padgett J (2017) Identification of the significant uncertain parameters in the seismic response of irregular bridges. *Eng Struct* 141:356–372.
<https://doi.org/10.1016/j.engstruct.2017.03.017>
- Soltanieh S, Memarpour MM, Kilanehei F (2019) Performance assessment of bridge-soil-foundation system with irregular configuration considering ground motion directionality effects. *Soil Dyn Earthq Eng* 118:19–34.
<https://doi.org/10.1016/j.soildyn.2018.11.006>
- Somala SN, Karthik Reddy KSK, Mangalathu S (2021) The effect of rupture directivity, distance and skew angle on the collapse fragilities of bridges. *Bull Earthq Eng* 19:5843–5869. <https://doi.org/10.1007/s10518-021-01208-8>
- Sullivan I, Nielson BG (2010) Sensitivity analysis of seismic fragility curves for skewed multi-span simply supported steel girder bridges. *Proc 19th Anal Comput Spec Conf* 226–237.
[https://doi.org/10.1061/41131\(370\)19](https://doi.org/10.1061/41131(370)19)
- Sun D, Dai J, Huang Y, Huang S (2023) Comparative experimental study on shaking table test of small radius curved bridge considering different connection types between pier and beam. *Structures*.
<https://doi.org/https://doi.org/10.1016/j.istruc.2023.105612>
- Tehrani P, Mitchell D (2013) Incremental dynamic analysis (IDA) applied to seismic risk assessment of bridges
- Terzic V, Stojadinovic B (2015) Calibration and Validation of Analytical Models for Predicting the Seismic and Axial-Load Response of Circular Bridge Columns. *J Bridg Eng* 20:04014098.
[https://doi.org/10.1061/\(asce\)be.1943-5592.0000702](https://doi.org/10.1061/(asce)be.1943-5592.0000702)
- Wen YK, Ellingwood BR, Veneziano D, Bracci J (2003) Uncertainty modeling in earthquake engineering. *MAE Cent Proj* 1–113
- Yang CSW, Werner SD, DesRoches R (2015) Seismic fragility analysis of skewed bridges in the central southeastern United States. *Eng Struct* 83:116–128. <https://doi.org/10.1016/j.engstruct.2014.10.025>
- Zakeri B, Ghodrati Amiri G (2014) Probabilistic performance assessment of retrofitted skewed multi span continuous concrete i-girder bridges. *J Earthq Eng* 18:945–963.
<https://doi.org/10.1080/13632469.2014.916241>
- Zakeri B, Padgett JE, Amiri GG (2014) Fragility Analysis of Skewed Single-Frame Concrete Box-Girder Bridges. *J*

Perform Constr Facil 28:571–582. [https://doi.org/10.1061/\(asce\)cf.1943-5509.0000435](https://doi.org/10.1061/(asce)cf.1943-5509.0000435)

Zakeri B, Zareian F (2018) Design of bridges with skewed abutments for a target tolerable seismic loss. Eng Struct 164:325–334. <https://doi.org/10.1016/j.engstruct.2018.02.020>